

Daily estimation of gross primary production under all sky using a light use efficiency model coupled with satellite passive microwave measurements

Yipu Wang ^a, Rui Li ^{a,b,c,*}, Jiheng Hu ^a, Yuyun Fu ^{a,c}, Jiawei Duan ^a, Yuanxi Cheng ^a

^a School of Earth and Space Sciences & State Key Laboratory of Fire Science, University of Science and Technology of China, Hefei 230026, China

^b Comparative Planetary Excellence Innovation Center, Chinese Academy of Sciences, Hefei 230026, China

^c Institut de recherche sur les forêts, Université du Québec en Abitibi-Témiscamingue (UQAT), Rouyn-Noranda J9X 5E4, Canada

ARTICLE INFO

Keywords:

Light use efficiency (LUE)
Gross primary production (GPP)
Satellite microwave
Emissivity Difference Vegetation Index (EDVI)
Cloudy sky

ABSTRACT

Although satellite-based light use efficiency (LUE) model is widely used to estimate gross primary production (GPP) of terrestrial ecosystems, microwave observations have not been integrated into LUE models. This study developed a new LUE model coupled with a passive microwave vegetation index (Emissivity Difference Vegetation Index, EDVI) for daily GPP estimation. Normalized EDVI (nEDVI), an indicator of canopy-scale leaf development and biomass change, was used as a proxy of fraction of photosynthetically active radiation (FPAR). EDVI-based evaporative fraction (EDVI-EF) under all sky was used to indicate synoptic-scale water stress on LUE. 8-year in-situ measurements from seven flux tower sites (four forests, two grasslands and one croplands) of ChinaFLUX network were used to evaluate the model. We found that nEDVI-based FPAR better captured the short-term variations in daily in-situ GPP (GPP_{obs}) than other optic-based FPAR schemes. This capability of nEDVI was more noticeable under moderate and heavy cloud cover (Frc) conditions. Validations against daily GPP_{obs} at all sites showed that EDVI-based GPP (GPP_{EDVI}) generated an overall small bias of $-0.47 \text{ gC m}^{-2} \text{ day}^{-1}$ (-8.1%) and good Taylor score (S) of 0.86 at the daily scale. Better accuracy of GPP_{EDVI} was found at forests sites with R^2 of 0.43 to 0.73, bias of 5.29% to 3.03% and S of 0.58 to 0.78, respectively. At a tropical forest site with most frequent cloud cover, the model also well captured the variation in GPP_{obs} from clear sky to cloudy sky (R^2 of 0.93) with stable accuracies. Furthermore, the accuracy of daily GPP_{EDVI} was found to be comparable with global satellite optic MOD17 GPP (GPP_{MOD17}) and EC-LUE GPP (GPP_{ECLUE}) from 8-day to yearly scales across the sites. In particular, GPP_{EDVI} performed generally smaller bias at evergreen broadleaf forests, while both of GPP_{MOD17} and GPP_{ECLUE} were overestimated, suggesting that there could be less saturation for microwave-based LUE model over dense vegetation. Although all three satellite LUE models severely underestimated GPP of crop, GPP_{EDVI} generated lower bias (-29.8%) than GPP_{MOD17} (-66.8%) and GPP_{ECLUE} (-59.5%). Overall, this study is the first attempt toward the integration of microwave-derived variables into LUE model for daily GPP estimation. The microwave-based LUE model has a potential of mapping spatiotemporally continuous daily GPP under various clouds.

1. Introduction

Terrestrial ecosystems fix atmospheric carbon dioxide (CO_2) through net photosynthesis and generate gross primary production (GPP). The process plays a critical role in the biochemical cycle of carbon between land and the atmosphere (Anav et al., 2015). GPP drives land carbon sequestration and partly offsets the anthropogenic CO_2 emission, which significantly affects global carbon balance and climate change (Janssens et al., 2003; Cox and Jones, 2008; Beer et al., 2010).

Local-scale GPP can be inferred from ecosystem respiration (RE) and net ecosystem exchange (NEE) measured by eddy covariance (EC) technique at flux tower stations (Reichstein et al., 2007). At a regional scale, however, direct measurements of NEE and GPP of ecosystems are difficult since associated processes cannot be quantified by current observation techniques (Ma et al., 2015). Satellite remote sensing can derive vegetation parameters related to photosynthesis, which makes regional and global GPP estimation possible.

Light use efficiency (LUE) model (Monteith, 1972, 1977) together

* Corresponding author at: School of Earth and Space Sciences & State Key Laboratory of Fire Science, University of Science and Technology of China, Hefei 230026, China.

E-mail address: rli7@ustc.edu.cn (R. Li).

with satellite remote sensing has been proved to be a powerful tool for deriving regional and global GPP (Xiao et al., 2004a, 2004b; Zhao et al., 2005; Yuan et al., 2010). Satellite LUE-based GPP estimation depends on fraction of absorbed photosynthetically active radiation (FPAR), the biophysical characteristics of vegetation as well as actual LUE converting radiation to the fixed carbon of plants. Most of satellite methods use optical vegetation indices (VIs) to quantify the characteristics of vegetation, such as the normalized difference vegetation index (NDVI), enhanced vegetation index (EVI) and leaf area index (LAI) (Xiao et al., 2004a, 2004b; Zhao et al., 2005; Sims et al., 2008; Yuan et al., 2010; Wu et al., 2009; Peng and Gitelson, 2012). Given that cloud and aerosol contaminations on optic signals (Samanta et al., 2010) as well as the various responses of vegetation physiology to cloud change (Knapp and Smith, 1988; Gu et al., 2003), an accurate representation of vegetation properties under clouds remains challenging.

Plant water status or water stress is a critical vegetation characteristic for stomatal and photosynthetic activity. In LUE models, water stress is typically used as a key controlling factor to down-regulate the maximum LUE to actual LUE for GPP estimation (Zhao et al., 2005; Yuan et al., 2007). Conventional models use soil moisture (SM) or vapor pressure deficit (VPD) to quantify the water stress on photosynthesis. Given that ecosystems fix carbon at the cost of plant inner water loss, such indication of SM or VPD may not accurately reflect the stress of plant inner water status on GPP generation. Although plant can be more sensitive to SM than VPD (Lyons et al., 2021), reliable SM products over large inhomogeneous surfaces remain lacked. Additionally, there also exists a time-lagged effect of vegetation in response to soil water deficit and atmospheric water demand from days to weeks (Zhang et al., 2016b; Liu et al., 2020). The accurate representation of water stress in current LUE models remains highly uncertain (Schaefer et al., 2012; Yuan et al., 2014; Zhang et al., 2015). Yuan et al. (2007, 2010) have shown that evaporative fraction (EF) can indicate the water stress on LUE more directly since it links the transpired water from plant to environments. Zhang et al. (2015) further indicated that LUE was more responsive to the change of plant moisture and EF than VPD and SM at the global scale. Thus plant moisture indicator can be the priority of quantifying water stress in LUE models.

Furthermore, water stress can be variable from clear sky to cloudy sky. From the perspective of vegetation-atmosphere interaction, clouds influence plant water loss via altering the incident radiation, surface wetness and temperature (Knapp and Smith, 1987, 1988; Berry et al., 2015; Schreel and Steppe, 2019). This would result in a fast response of vegetation to the varying environmental conditions (Jones, 1998). For instance, Knapp and Smith (1988) illustrated that a water-stressed herbaceous perennial produced more rapid stomatal response than the riparian herb with less water stress under various cloud patterns. The water-stressed species typically maintained a higher water use efficiency in photosynthesis during cloud cover periods (Knapp and Smith, 1988). Rocha et al. (2004) reported that the photosynthesis of a temperate hardwood forest under clear sky was more limited by lower soil moisture than higher soil moisture, while such limitation due to the soil moisture deficit was insensitive under overcast sky. Therefore, the accurate representation of water stress conditions under clouds appears to be crucial for GPP estimation at a short term scale (e.g. daily or weekly scales).

From the perspective of satellite remote sensing, most of satellite vegetation observations depending on optic sensors leads to the difficulty in capturing the synoptic-scale variations of plant water stress associated with clouds. In contrast, satellite microwave observations with longer wavelength are competent for the direct monitoring of vegetation status under clouds (Konings et al., 2019). Also, owing to the high dielectric properties of water (Ulaby et al., 1990), the attenuation of microwave radiation at different wavelengths when penetrating vegetation canopy layers is highly sensitive to the total biomass and vegetation water content (VWC) (Liu et al., 2015; Tian et al., 2016; Rodríguez-Fernández et al., 2018; Teubner et al., 2018). These features make them have a great potential for GPP estimation under the impact of

clouds. Alternatively, microwave VIs are important tools to quantify the synoptic-scale plant water availability. Several microwave VIs have been proposed, such as microwave polarization difference index (MPDI) (Becker and Choudhury, 1988; Paloscia and Pampaloni, 1992), microwave vegetation index (MVI) (Shi et al., 2008), microwave Emissivity difference vegetation index (EDVI) (Min and Lin, 2006a, 2006b) and microwave vegetation optical depth (VOD) (Teubner et al., 2018, 2019). Among them, VOD has been used in GPP estimation (Teubner et al., 2018, 2019) and other GPP-related studies (Liu et al., 2015; Momen et al., 2017; Tian et al., 2016; Rodríguez-Fernández et al., 2018). In spite of that, the implement of microwave in LUE-based GPP models remains lacked.

Satellite microwave EDVI was proposed and developed in recent years (Min and Lin, 2006a, 2006b; Li et al., 2020). Early studies have proved that EDVI as a vegetation water index is sensitive to the change of VWC and has a significantly statistical correlation with carbon uptake flux in a middle latitude forest (Min and Lin, 2006a). EDVI can also accurately monitor the hydrological status and volatile organic compounds of Amazon forests under various cloud conditions (Min et al., 2010; Li and Min, 2013; Zhang et al., 2019). Our recent studies have used EDVI to map the VWC status under clouds (Li et al., 2020) and to study water exchange between ecosystems and atmosphere over East Asia (Wang et al., 2019a, 2019b; Li et al., 2009). It also has been illustrated that the energy partitioning for transpired plant water under clouds can be quantified by EDVI-based schemes. Specifically, normalized EDVI (i.e. relative change of EDVI in growing seasons) has been found to be able to monitor the plant phenology and biomass development (Min and Lin, 2006b). These studies suggest that EDVI has a potential for the quantitative estimation of GPP.

Accordingly, this study attempts to develop a daily satellite GPP model based on LUE framework coupled with microwave EDVI and EDVI-derived variables. The specific objectives are as follows: 1) to evaluate the performance of EDVI-based FPAR scheme and LUE model (EDVI-LUE) using in-situ measurements and other satellite optic indices across seven forests, grass and crop sites of ChinaFLUX; 2) to test the ability of satellite microwave-based model for daily GPP estimation under clouds; 3) to intercompare EDVI-LUE model with widely used MOD17 GPP and EC-LUE GPP products at multiple temporal scales. The structures of this study are as follows: Section 2 described the data sources in this study; Section 3 showed the description of EDVI-based LUE model; Section 4 displayed the results from our GPP estimations and the comparisons with other two satellite GPP products. Section 5 discussed the uncertainties in our model and Section 6 made conclusions.

2. Data

2.1. In-situ measurements

Seven flux tower sites of ChinaFLUX network were used in this study (Fig. 1). Table 1 provided the basic information of the sites (Yu et al., 2006, 2008). The flux tower sites use eddy covariance (EC) method to measure carbon and water fluxes between ecosystem and the atmosphere. Five major vegetation types are included at the sites: evergreen broadleaf forest (BNS, DHS), evergreen needleleaf forest (QYZ), mixed forest (CBS), grass (QHB) and crop (YCS). The site environments are affected by East Asia monsoon. Annual mean air temperature (Ta) and precipitation (P) range from -1.7°C to 21.8°C and from 351 mm to 1956 mm, respectively. Cloud cover (Frc) presents frequently over the sites. Mean fractional Frc during May to October varies from 17.5% to 36.8%. South forest sites (BNS, DHS and QYZ) are severely covered by clouds. Clear days (Frc < 10%) only account for 18.3% at BNS, 22.5% at DHS and 25.4% at QYZ, respectively (Table 1). More site information can be found at ChinaFLUX website (<http://www.chinaflux.org>) and in Yu et al. (2006, 2008).

Each site provided the standard 30 min measurements of net

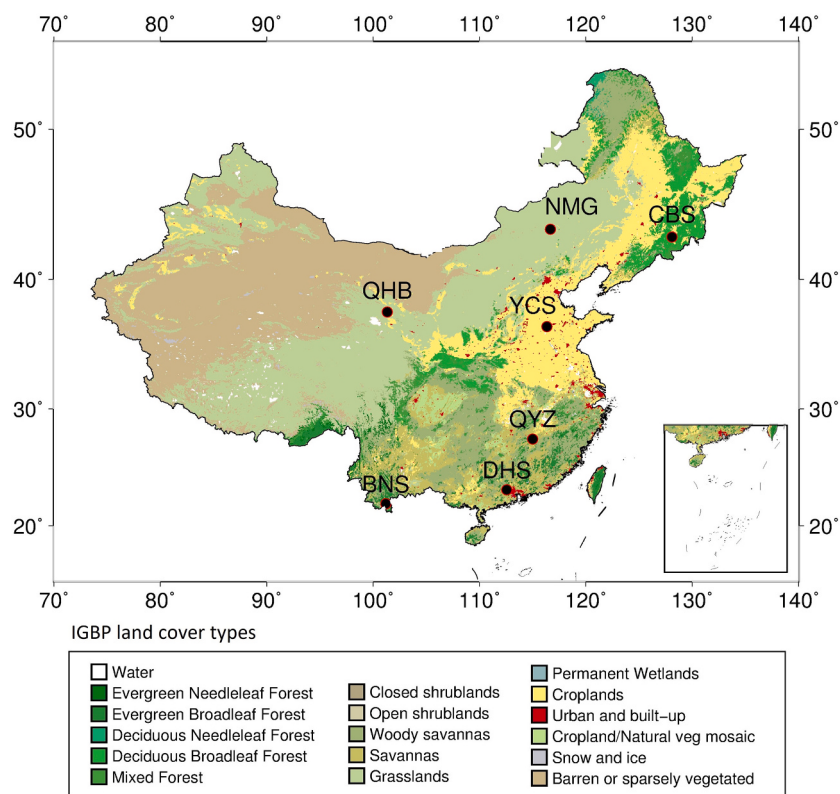


Fig. 1. Locations of seven flux tower sites in this study. Land cover types are obtained from the International Geosphere-Biosphere Programme (IGBP) types of MCD12C1 product.

Table 1
Site information (Yu et al., 2006, 2008).

Sites	IGBP	Latitude (°)	Longitude (°)	Elevation (m)	Climate ^a	Ta ^b (°C)	P ^b (mm)	Frc ^c (%)	Proportion of clear days ^d (%)	Study period (2003–2010)
BNS	EBF	21.928	101.265	756	Af	21.8	1493	32.5	18.3	Jan.to Dec.
DHS	EBF	23.167	112.567	300	Am	20.9	1956	36.8	22.5	Jan.to Dec.
QYZ	ENF	26.734	115.066	102	Am	17.9	1542	34.2	25.4	Jan.to Dec.
CBS	MF	42.403	128.096	738	Cfc	3.6	713	24.4	38.8	May. to Oct.
QHB	GRA	37.60	101.35	3327	Bsk	-1.7	580	24.6	36.9	May. to Oct.
NMG	GRA	43.55	116.667	1189	Bsk	0.4	351	17.5	52.9	May. to Oct.
YCS	CRO	36.83	116.57	28	Dwa	13.1	610	27.2	37.8	Mar. to Oct.

^a Climates are Köppen-Geiger climates (Kottek et al., 2006). Af is equatorial and fully humid climate; Am is equatorial and monsoonal climate; Bsk is arid, steppe and cold climate; Cfc is warm temperate, fully humid and cold summer climate; Dwa is snow, desert and hot summer climate.

^b Ta and P are annual mean air temperature and precipitation.

^c Mean cloud cover was calculated from daily MODIS cloud cover data (MYD06) during May to October.

^d Clear days are the days with cloud cover less than 10%.

ecosystem CO₂ exchange (NEE, mg CO₂ m⁻² s⁻¹), incoming shortwave radiation (SW_{in}, W m⁻²) and air temperature (Ta, °C). Ecosystem respiration (RE, mg CO₂ m⁻² s⁻¹) was estimated using the Lloyd-Taylor partitioning method and officially provided (Taylor, 1994; Wang et al., 2015; Gui et al., 2021). Daily total GPP can be thus derived using 30 min RE and NEE data (Eq. 1).

$$\text{Daily GPP} = \sum (\text{RE}_{30\text{min}} - \text{NEE}_{30\text{min}}) \quad (1)$$

In-situ measured 30 min SW_{in} within a day was integrated into daily total SW_{in} (MJ day⁻¹). The averaged Ta during daytime (i.e. SW_{in} > 0 W m⁻²) was used. The two variables were used as radiation and temperature inputs into LUE model.

2.2. EDVI and normalized EDVI

Satellite EDVI was defined as the normalized difference between microwave land surface emissivity (MLSE) at 18.7 and 36.5 GHz (Eq. 2),

which is strongly related to vegetation vertical structures and VWC (Min and Lin, 2006a, 2006b; Li et al., 2020). In combination with AMSR-E microwave and MODIS optic observations, our recent study established the latest all-sky EDVI dataset at daily temporal resolution and at ~20 km resolution over East Asia (Li et al., 2020). This study used the latest EDVI datasets as a key input of vegetation properties. The details of satellite retrieval of EDVI can be found in Li et al. (2020).

$$\text{EDVI} = \frac{\text{MLSE}^{18.7} - \text{MLSE}^{36.5}}{0.5(\text{MLSE}^{18.7} + \text{MLSE}^{36.5})} \quad (2)$$

EDVI normalized by its minimum and maximum values during a vegetation growing period (i.e. nEDVI) represents the relative change of EDVI from its spring onset (Eq. 3). nEDVI is a good indicator of canopy leaf development during a leaf growing stage, which depends on the change of total biomass. It has been well used to monitor the seasonal changes of total biomass and to detect canopy phenology within uncertainty of 3–7 days (Min and Lin, 2006b).

$$nEDVI = \frac{EDVI - EDVI_{min}}{EDVI_{max} - EDVI_{min}} \quad (3)$$

Where $EDVI_{min}$ is the minimum EDVI of vegetation at spring onset. $EDVI_{max}$ is the maximum EDVI during a middle growing season when vegetation generates the maximum exchange of water and carbon with surrounding environments. $EDVI_{min}$ and $EDVI_{max}$ depend on biome types and local environments (Li et al., 2009; Wang et al., 2019a), which can be determined by the amplitude of seasonal variations in EDVI. In this study, we determined $EDVI_{min}$ and $EDVI_{max}$ based on the EDVI at 5th and 95th percentiles at each site. As shown in Fig. 2, for example, we first resorted EDVI from the lowest to the highest and investigated its probability distribution function (PDF) as well as cumulative density function (CDF). The averaged value for the EDVI lower than 5th percentile was used as the base line (i.e. $EDVI_{min}$), while the averaged value for the EDVI larger than 95th percentile was used as the upper line (i.e. $EDVI_{max}$) (Fig. 2a). It should be notified that heavy precipitation events during a short period could reduce microwave signals from vegetation, which might result in abnormally small EDVI and thereby $nEDVI$ (Li et al., 2020). The estimated $nEDVI$ was thus set to be 0.1 when EDVI was lower than $EDVI_{min}$ and to be 1.0 when EDVI was larger than $EDVI_{max}$. This setting may partly reduce uncertainties due to the EDVI outliers.

2.3. Satellite GPP products

Two global satellite GPP products based on LUE model were used for comparison. One is global MOD17 GPP (GPP_{MOD17}) which is 8-day composite product at 500 m resolution (Zhao et al., 2005; Running and Zhao, 2019). The product was driven by MODIS land cover, MODIS LAI/FPAR and surface meteorological data from NASA GMAO (the Global Modeling and Assimilation Office). In GPP_{MOD17} model, the stress functions of minimum Ta and VPD were used to reduce maximum LUE

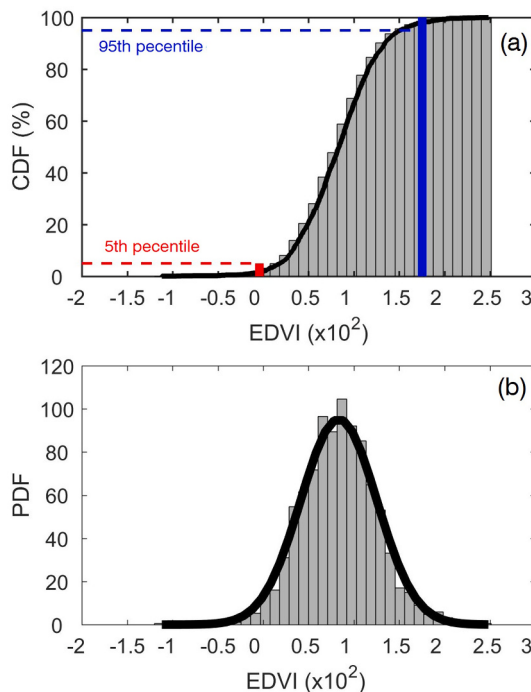


Fig. 2. An example of determining the minimum EDVI and the maximum EDVI using the percentile method at BNS site. (a) Cumulative density function (CDF) and (b) probability density function (PDF) of EDVI samples in growing seasons from 2003 to 2010. The red and blue vertical lines stand for the EDVI at 5th and 95th percentiles, respectively. (For interpretation of the references to colour in this figure legend, the reader is referred to the web version of this article.)

to actual LUE. The issue of cloud contamination on MODIS inputs was corrected using temporal interpolation method (Zhao et al., 2005). GPP_{MOD17} product has been widely used in the study of ecosystem productivity. It can be available at the website (<https://lpdaac.usgs.gov/>).

The other satellite GPP product was from global EC-LUE GPP model (Yuan et al., 2010). The published global EC-LUE GPP product (GPP_{ECLUE}) has 8-day and 0.05° resolution. The model was driven by vegetation products from MODIS LAI and NDVI, and satellite radiation product from GLASS (the Global Land Surface Satellite). To quantify the water stress on LUE, the model used evaporative fraction (EF) which was derived from RS-PM (remote sensing-Penman Monteith) ET method of Mu et al. (2007) and surface net radiation (Rn) of GLASS, i.e. EF = ET/Rn. GPP_{ECLUE} dataset is available at the GLASS website (<http://www.glass.umd.edu/Download.html>).

2.4. Ancillary data

To help analyze our results, other ancillary MODIS datasets were used in this study, including cloud cover from MYD06 (daily and 5 km resolution), NDVI from MYD13C1 (16-day and 0.05° resolution) and FPAR/LAI from MYD15A1 (8-day and 500 m). They were obtained from MODIS website (<https://modis.gsfc.nasa.gov/data/dataproducts/>). In order to minimize cloud contamination on MODIS vegetation data, we first used the quality control (QC) of cloud state layers to screen the data. Only the reliable MODIS pixels distinguished by “clear sky” (e.g. QC of 0 or 3 in the CloudState layer of FPAR) were used. In spite of this, there remained some abnormal values which could not be distinguished by MODIS QC, i.e. cloud-contaminated data with good QC label (Running and Zhao, 2019). NDVI and FPAR/LAI data were further filtered by using Savitzky-Golay filter which was a widely used time series reconstruction method for cloud-contaminated optic data (Zhou et al., 2016; Wang et al., 2018). Then filtered data were linearly interpolated into daily values.

For the data collocation and validation at each site, a 0.15° × 0.15° box area covered with similar land cover types surrounding each site was selected, as we did in Wang et al. (2019a), which may partly reduce the influence of surface inhomogeneity within the area. All of the original satellite datasets were averaged within the selected area and then area-averaged data were collocated on each day of year.

2.5. Metrics for model evaluation

Several conventional statistical metrics were used to evaluate model performance, including bias, Pearson correlation coefficient (R), determination coefficient (R^2) and root mean squared error (RMSE). Bias and RMSE have the same unit as GPP (i.e. gC m⁻² day⁻¹). The relative bias (the ratio of bias to the mean value, in unit of %) and the relative RMSE (the ratio of RMSE to the mean value, in unit of %) were also used. Furthermore, Taylor (2001) indicated that RMSE might be inadequate for evaluating a model skill comprehensively and thus proposed the comprehensive Taylor Score (S). S is defined by standard deviation (σ) and R between in-situ measurements and calculations (Taylor, 1994):

$$S = \frac{4 \times (1 + R)}{(\bar{\sigma} + 1/\bar{\sigma})^2 \times (1 + R_{max})} \quad (4)$$

Where R_{max} is the maximum R (i.e. $R_{max} = 1.0$). $\bar{\sigma}$ is the standard deviation of estimation normalized by the standard deviation of observation ($\sigma_{est}/\sigma_{obs}$). S typically varies from 0 (poorest performance) to 1 (best performance). S has been used in model evaluation (Yao et al., 2017; Velpuri et al., 2013).

3. Description of EDVI-based LUE model

Light use efficiency model can be simply expressed as in Eq. (5). The

process of plant photosynthesis is regulated jointly by radiation situations and vegetation properties. EDVI is directly related to the controlling factors of photosynthetic activity (e.g. vegetation moisture status, radiation use efficiency) (Min and Lin, 2006a, 2006b). nEDVI is a good indicator of the seasonal change of canopy leaf physiology and carbon uptake. Early study has shown that the correlation between forest CO₂ uptake flux and the product of PAR and EDVI was statistically significant (Min and Lin, 2006b). This means that incident radiation could be downregulated by EDVI-derived variables for carbon uptake in canopy photosynthesis. On the other hand, the biosynthesis of chlorophyll can be affected by inner VWC. The deficit in VWC may increase the decomposition of leaf chlorophyll and induce the closure of stomata, which can lead to the decline in photosynthetic activity and thus decrease the absorption of CO₂ and PAR (Cornic, 2000; Flexas and Medrano, 2002; Damm et al., 2018). These findings suggested that EDVI and EDVI-derived variables might be useful in GPP estimation.

$$GPP = APAR \times LUE \quad (5)$$

Where APAR is the PAR absorbed by vegetation canopy and can be estimated by FPAR. LUE is the actual LUE used for GPP.

3.1. Absorbed photosynthetically active radiation

LUE model assumes a linear correlation between GPP and FPAR on a canopy or ecosystem scale. The estimation of FPAR depends on vegetation types and vegetation cover conditions. Generally, FPAR can be estimated empirically using a linear relationship with NDVI (e.g. FPAR = 1.24NDVI - 0.168) (Waring et al., 1995; Sims et al., 2005; Myneni and Williams, 1994), or the Beer-Lambert law based on LAI (e.g. FPAR = 1 - e^{-0.5LAI}) (Ruimy et al., 1999; Xiao et al., 2004a).

Since nEDVI strongly correlates with plant phenology and the development of total biomass in a growing season (Min and Lin, 2006b), the index also can be used to indicate the change of canopy-scale FPAR. For example, Fig. 3 showed seasonal variations in daily GPP_{obs}, nEDVI, NDVI and MODIS FPAR. Seasonal nEDVI was found to agree well with GPP_{obs} (R^2 of 0.59 to 0.92) at the sites. The patterns of nEDVI at the sites were close to those of NDVI (R^2 of 0.49 to 0.88) and FPAR (R^2 of 0.15 to 0.89), illustrating the consistent changes of seasonality in VWC, canopy chlorophyll content and total biomass. In comparison, nEDVI of forests displayed more noticeable seasonal amplitudes than NDVI and FPAR, particularly at evergreen forests (BNS and DHS) where NDVI and FPAR were typically saturated in middle-growing seasons (Fig. 3a,b). Higher temporal correlation ($R^2 > 0.67$) between nEDVI and GPP_{obs} than those ($R^2 < 0.62$) for NDVI and for FPAR implied that microwave nEDVI might better capture the seasonal variations in canopy-scale GPP of dense forests due to the deeper penetration and less saturation of microwave signals than optic signals. Particularly, YCS crop site displayed unique bimodal peaks in GPP_{obs} because of the growth of winter wheat and summer maize, which was also captured by nEDVI.

Furthermore, daily variations in GPP_{obs} were found to be noticeable, which potentially indicated the changeable absorption of PAR for developing chlorophyll and biomass at the short term scale. Such short-term variations in GPP_{obs} were affected by atmospheric conditions (e.g. cloud cover, incident radiation and CO₂ concentration) and vegetation properties (e.g. stomata aperture, plant water status). nEDVI was found to capture the GPP_{obs} variations across forest and crop sites (e.g. BNS, CBS, YCS Fig. 3a,d,f), especially in middle-growing seasons when vegetation fully developed, while daily NDVI and FPAR derived from Savitzky-Golay filtering performed more smoothly. Under various Frc conditions (Fig. 4), nEDVI was further found to have a higher correlation with GPP_{obs} than other optic indices at the daily scale. This was more noticeable for moderate and high Frc (>50%) when correlation between optic indices and GPP_{obs} declined. The result implied that although the optic NDVI/LAI/FPAR under clouds could be derived by filtering or temporal interpolation based on their clear-sky values, it remained

difficult for them to capture the fast change of GPP affected by clouds.

Based on these results, we designed the following formula as the approximation of APAR at an ecosystem scale:

$$APAR = SW_{in} \times 0.45 \times nEDVI^K \quad (6)$$

$$nEDVI = \begin{cases} 0.1 & nEDVI < 0.1 \\ nEDVI & 0.1 \leq nEDVI \leq 1.0 \\ 1.0 & 1.0 < nEDVI \end{cases} \quad (7)$$

Where SW_{in} is the daily total incident shortwave radiation (MJ m⁻² day⁻¹). nEDVI^K is the approximation of FPAR. K is the adjusted factor indicating the sensitivity of GPP to APAR partitioned by nEDVI over different biome types. In this study, K was determined at each site when daily GPP_{obs} and the nEDVI-based APAR (Eq. 6) reached a highest correlation in the growing seasons (Table 2). Eq. (7) indicated the range of variation in nEDVI with the underlying assumptions that: (a) a surface with EDVI ≤ EDVI_{min} has weak vegetation growth and photosynthesis, (b) a surface with EDVI ≥ EDVI_{max} has full canopy leaf development with large amount of VWC and strong photosynthesis in middle growing seasons, and (c) canopy-scale APAR for GPP increases linearly with nEDVI^K at an intermediate EDVI (Eq. 3; Fig. 2).

Fig. 5 showed the comparison of different FPAR schemes based on nEDVI (FPAR_{nEDVI}), NDVI (FPAR_{NDVI}, Sims et al., 2005), MODIS FPAR (FPAR_{MOD}) and LAI (FPAR_{LAI}, Xiao et al., 2004a). FPAR_{nEDVI} was found to strongly correlate with daily GPP_{obs} (R^2 of 0.95) across the sites (Fig. 5a). The performance was overall better than optic FPAR schemes (R^2 of 0.64 to 0.83). Owing to the saturation of optic signals, most of optic FPAR samples distributed in the high biomass level (e.g. GPP > 5 gC m⁻² day⁻¹, FPAR > 0.6) (Fig. 5b,c,d), leading to the relatively lower sensitivity of GPP to optic FPAR schemes (slopes of 6.0 to 8.33). In contrast, GPP_{obs} performed a larger sensitivity to the microwave FPAR_{nEDVI} (slope of 10.2) with less saturation. Overall, these results illustrated the applicability of nEDVI as indicator of FPAR.

3.2. Light use efficiency

Vegetation typically generates the maximum LUE (LUE_{max}) under an optimum condition. In general, LUE_{max} can be converted into the actual LUE for the GPP estimation via the regulation of environmental and biophysical stress. In this study, we took environmental air temperature and vegetation moisture stress as the two most important stress factors on LUE_{max}, i.e. thermal stress and plant inner water stress (Ws). The Liebig's law indicated that actual LUE can be determined by the most limiting factor during a growing season (Yuan et al., 2007). We thus adopted this law in this study (Eq. 8).

$$LUE = LUE_{max} \times \text{Min}(f(Ta), f(Ws)) \quad (8)$$

Where f(Ta) and f(Ws) range from 0 (complete inhibition) to 1 (no inhibition). LUE_{max} (g C m⁻² MJ⁻¹ APAR) represents the maximum LUE of absorbed PAR being converted into GPP under an optimum condition. LUE_{max} is generally taken as a biome-specific physiological constant. We used the optimized LUE_{max} at the ChinaFLUX sites from the study of Wang et al. (2015) who used evolution algorithm to derive optimum LUE_{max} with the consideration of diffuse radiation effect (Table 2).

The change of air temperature can regulate the stomatal activity and carbon uptake. The equation of Jarvis (1976) was used to quantify the stress of Ta on plant stomatal activity, such that:

$$f(Ta) = \left(\frac{Ta - Ta_{min}}{Ta_{opt} - Ta_{min}} \right) \left(\frac{Ta_{max} - Ta}{Ta_{max} - Ta_{opt}} \right)^{\left(\frac{Ta_{max} - Ta_{opt}}{Ta_{opt} - Ta_{min}} \right)} \quad (9)$$

Where Ta is the average temperature during daytime. Ta_{min} and Ta_{max} are minimum (2.7 °C) and maximum (45.3 °C) temperature for stomatal activity, respectively (Nishida et al., 2003). The various optimal temperature (Ta_{opt}) for photosynthesis of ecosystems was used at the sites

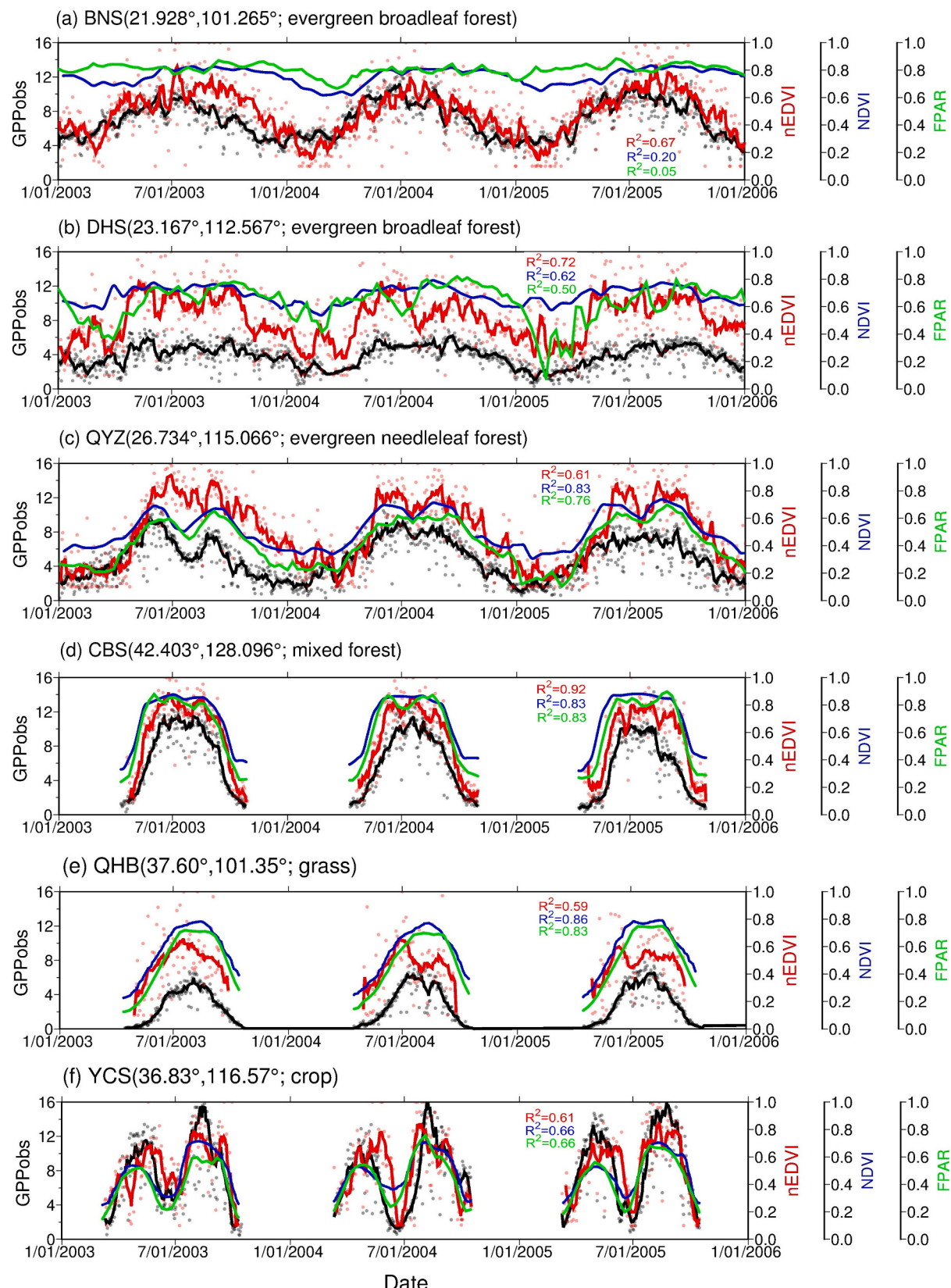


Fig. 3. Time series of daily in-situ GPP (GPP_{obs} , black), normalized EDVI (nEDVI, red), NDVI (blue) and FPAR from MYD15 product (green). Black dots and black curves stand for daily GPP_{obs} and 8-day moving average daily GPP_{obs} , respectively. Red dots and red curves stand for original daily nEDVI and 8-day moving average daily nEDVI, respectively. NDVI and FPAR are daily values filtered by Savitzky-Golay filter method. R^2 shows the correlation between GPP_{obs} and indicators. (For interpretation of the references to colour in this figure legend, the reader is referred to the web version of this article.)

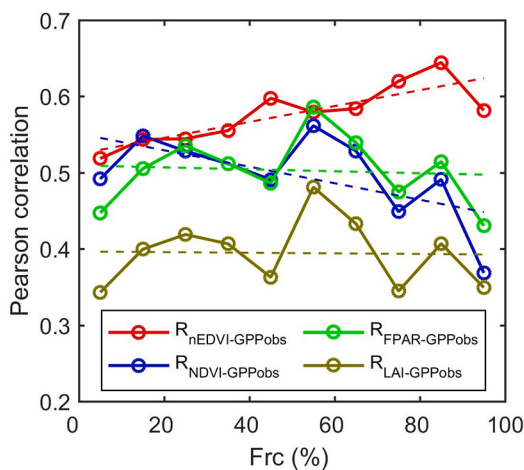


Fig. 4. Pearson correlation between daily GPP_{obs} and different indices under various cloud cover (Frc). Dashed lines indicate the linear trend in the correlation with increase of Frc. The correlation was conducted over all sites at the daily scale.

Table 2

Parameters used in EDVI-based GPP model at the sites.

Sites	IGBP	EDVI _{min} ^a	EDVI _{max} ^a	K ^a	LUE _{max} ^b	Ta _{opt} ^c
BNS	EBF	-0.0004	0.0175	0.8	2.463	25.1
DHS	EBF	-0.0120	0.0095	1.2	2.087	27.8
QYZ	ENF	-0.0128	0.0117	0.5	2.676	26.8
CBS	MF	-0.0115	0.0142	1.5	3.867	22.0
QHB	GRA	-0.0109	0.0115	1.0	1.61	12.3
NMG	GRA	-0.0102	0.0129	0.5	0.838	17.7
YCS	CRO	-0.0106	0.0135	1.5	2.453	25.9

^a EDVI_{min}, EDVI_{max} and K were determined at each site in the study periods from 2003 to 2010: January to December at BNS, DHS and QYZ, May to October at CBS QHB and NMG, March to October at YCS.

^b The optimized LUE_{max} by Wang et al. (2015).

^c The optimized Ta_{opt} by Yang et al. (2021).

(Table 2, Yang et al., 2021). The values of Ta_{opt} were determined by the response curve of ecosystem-scale EVI to Ta in growing seasons. The estimated Ta_{opt} have been validated by the temperature response curve of the maximum GPP at the sites (Yang et al., 2021).

Plant water stress on LUE can be quantified by evaporative fraction (EF) and evapotranspiration (ET) which represent the transpired water loss from internal plant to atmosphere (Yuan et al., 2007, 2010). Given that most of current satellite ET methods are derived from optic observations which are limited to clear sky conditions (Wang and Dickinson, 2012; Zhang et al., 2016a), we have developed a satellite microwave method to directly estimate EF of vegetation (EF_{veg}) under cloud cover (Wang et al., 2019a, 2019b; Li et al., 2009).

$$f(Ws) = EF_{veg} \quad (10)$$

$$EF_{veg} = \frac{\alpha\Delta}{\Delta + \gamma(1 + Ga/2Gc)} \quad (11)$$

where α is the Priestley-Taylor's parameter (1.26), γ is the psychometric constant (0.0665 kPa/°C), Δ is the slope of saturated vapor pressure at air temperature, kPa/°C. Ga is the aerodynamic conductance determined by canopy surface air density and air temperature (Mu et al., 2011; Thornton, 1998). Gc is the canopy conductance which is the summation of the cuticle conductance (10^{-5} ms^{-1}) and stomatal conductance within a whole canopy ($Gc_{stamata}$). The method used normalized EDVI as an indicator of canopy phenology to constrain the maximum stomatal conductance during growing seasons (Eq. (12)). Day-to-day variations in EDVI was used to quantify the combined effect

of atmospheric demand (i.e. VPD), plant water potential (ψ) and ambient carbon dioxide concentration (i.e. CO₂) on canopy conductance (i.e. $F(\text{VPD}, \psi, CO_2)$, Eq. (13)). This quantification indicates the fast response of Gc due to variations in canopy water status associated with sky and environmental conditions (Li et al., 2009).

$$Gc_{stamata} = Gc_{max} \times nEDVI \times f(Ta) \times f(PAR) \times F(\text{VPD}, \psi, CO_2) \quad (12)$$

$$F(\text{VPD}, \psi, CO_2) = [b - a \times (EDVI_i - EDVI_{i-1})]^{-1} \quad (13)$$

In which Gc_{max} is the biome-specific maximum canopy conductance (i.e. minimum canopy resistance) during growing seasons (Kelliher et al., 1995; Wang et al., 2019a). $f(Ta)$ and $f(PAR)$ are constraints of air temperature and radiation on stomatal activity, respectively. i indicates a day of a year. a and b are coefficients (Li et al., 2009). These schemes have been found to be effective for estimating plant transpiration under all sky over different vegetation types (Wang et al., 2019a). This also suggests that EDVI-based EF_{veg} could be used to represent the synoptic-scale moisture stress due to the change of vegetation inner water under cloud impact in the LUE model.

4. Results

4.1. Comparison of daily GPP estimation from different FPAR schemes

Fig. 6 showed the validations of daily GPP estimations using different FPAR schemes. FPAR_{nEDVI}-based GPP (GPP_{EDVI}) was found to have the R^2 of 0.52 and RMSE of 46.4% for all site estimations (Fig. 6a). The metrics were found to be better than those of FPAR_{NDVI}-based GPP (GPP_{NDVI}), FPAR_{MOD}-based GPP (GPP_{FPAR}) and FPAR_{LAI}-based GPP (GPP_{LAI}) (R^2 of 0.40 to 0.45, RMSE of 58.1% to 67.6%), respectively. Scatters of GPP_{EDVI} were closer to 1:1 line with less scattering than those of other GPP estimations. The bias of GPP_{EDVI} ($-0.47 \text{ gC m}^{-2} \text{ day}^{-1}$ or -8.1%) was also found to be comparable with those of other FPAR-based GPP (5.5% to 14.5%). The higher S for GPP_{EDVI} (0.86) (Fig. 6a) further indicated that EDVI-based LUE model coupled with FPAR_{nEDVI} was effective for daily GPP estimation under all sky.

At different sites, GPP_{obs} displayed significant seasonal variations and amplitudes (Fig. 7), typically increasing from low values ($<4 \text{ gC m}^{-2} \text{ day}^{-1}$) in spring to the maximum ($>8 \text{ gC m}^{-2} \text{ day}^{-1}$) in summer and then decreasing in autumn and winter. This pattern of GPP_{obs} was found to be well captured by GPP_{EDVI} at most of sites, with fairly good temporal R^2 of 0.42–0.73 (Table 3, except for NMG), demonstrating that the EDVI-LUE model was able to simulate the seasonality of GPP for the ecosystems. Among the sites, GPP_{EDVI} performed a better seasonal consistency with GPP_{obs} (R^2 of 0.43–0.73) at four forest sites (i.e. BNS, DHS, QYZ, CBS) and highland grass site (i.e. QHB) (Fig. 7a–e) than at north grass (NMG) and crop (YCS) sites (R^2 of 0.07 to 0.42) (Table 3).

Statistic results showed that GPP_{EDVI} generated lower bias of -0.28 to $0.2 \text{ gC m}^{-2} \text{ day}^{-1}$ (-5.29% to 3.03%) at four forest sites than other sites (Table 3). Although the daily model underestimated GPP_{EDVI} by $0.90 \text{ gC m}^{-2} \text{ day}^{-1}$ (17.1%) at QHB and by $2.89 \text{ gC m}^{-2} \text{ day}^{-1}$ (31.0%) at YCS sites, respectively, it was still found to have good S of 0.84 and 0.71 at the two sites. At NMG site, GPP_{EDVI} was overestimated by $0.92 \text{ gC m}^{-2} \text{ day}^{-1}$ (45.7%) with relatively lower S of 0.51.

Furthermore, it can be found that clouds presented frequently (Frc of 20% to 100%) throughout growing seasons at the sites. The fast change of Frc remarkably caused some short-term fluctuations in GPP_{EDVI} via altering the incident solar radiation which was the key driving force of the model (Eq. 5). This performance agreed with GPP_{obs} and suggested that cloud effect could be significant for satellite GPP estimation at the daily scale. In addition, at the middle latitude sites (e.g. CBS, QHB, YCS), some underestimated peaks in GPP_{EDVI} were found in middle-growing seasons with the heaviest Frc (Fig. 7d,e,f,g), which led to the overall underestimations of GPP_{EDVI} (Table 3).

Compared to other optic FPAR-based GPP, GPP_{EDVI} generated significantly better accuracy for the evergreen broadleaf forest (BNS,

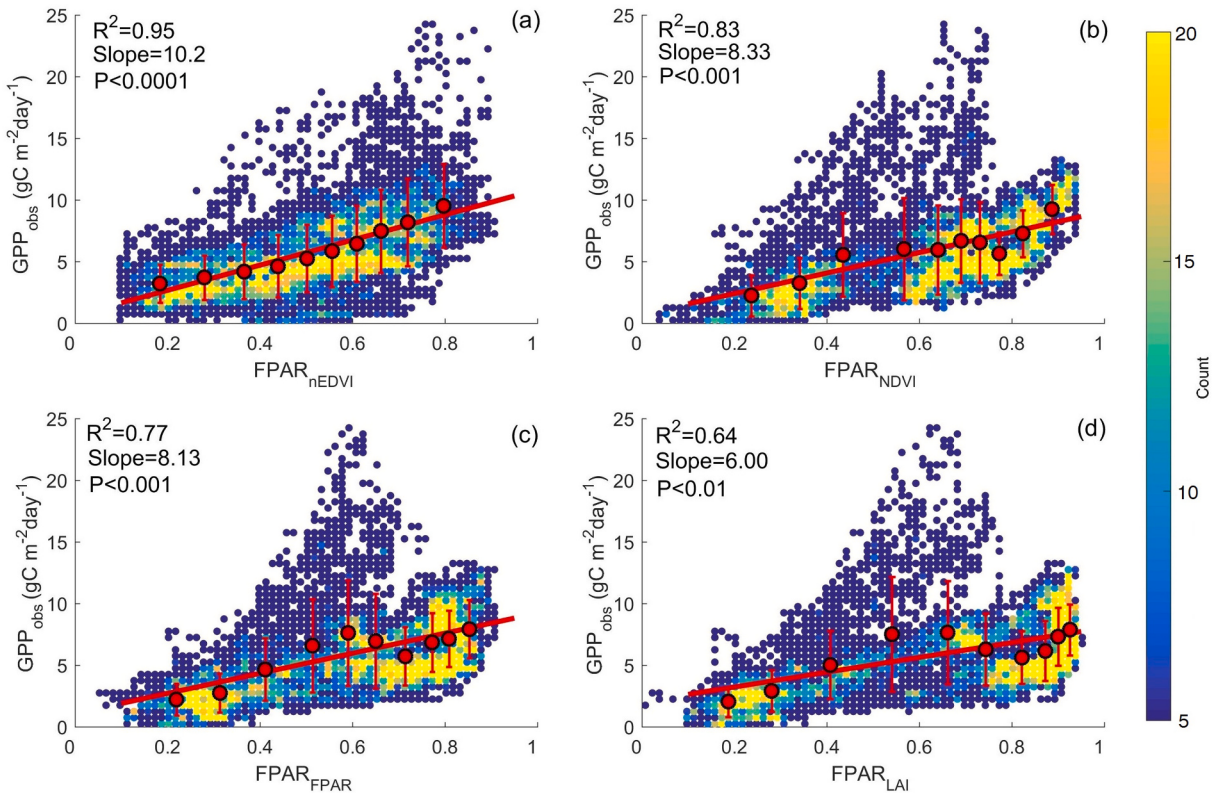


Fig. 5. Comparisons of daily FPAR estimated from (a) nEDVI, (b) NDVI ($\text{FPAR}_{\text{NDVI}} = 1.24\text{NDVI} - 0.168$), (c) MODIS FPAR product and (d) LAI ($\text{FPAR}_{\text{LAI}} = 1 - e^{-0.5\text{LAI}}$) across the sites. Red spots are averaged values in each bin of 0.1. Error bars represent standard deviations. The blue and yellow colour stands for low and high density of scatters, respectively. The slopes of linear fitting lines and statistical results were calculated using bin-averaged FPAR and GPP_{obs} . (For interpretation of the references to colour in this figure legend, the reader is referred to the web version of this article.)

DHS) and mixed forest (CBS) (Table 3), as indicated by lower bias, smaller RMSE and higher S. GPP_{NDVI} , GPP_{FPAR} and GPP_{LAI} were found to be overestimated by 29.6% to 60.2% with lower S (0.36 to 0.62) at the three sites. Most of those overestimations presented in the transient period (November to May) (Fig. 7 a, b), which could be related to the saturation in NDVI and LAI over the forests. GPP_{EDVI} at QYZ site performed a noticeably smaller bias than other three GPP estimations (bias of -28.9% to -35.6%), although the latter had slightly better S. At grass (QHB, NMG) and crop (YCS) sites, GPP_{EDVI} was found to have better or comparable scores (0.51 to 0.84) than GPP_{NDVI} , GPP_{FPAR} and GPP_{LAI} (0.26 to 0.84) (Table 3), while larger errors and lower temporal correlation for GPP_{EDVI} indicated a relatively larger uncertainty in microwave signals than optic signals for GPP estimation over shortly vegetated surfaces.

Further investigation also found that performances of EDVI-LUE model at the sites were comparable to existing GPP models. For example, Liu et al. (2014) compared six satellite GPP models at the same sites we selected in this study. They showed that the 8-day GPP models generally had R^2 of 0.16–0.34 and RMSE of 42.9%–72.8% at BNS and DHS sites, while the models performed R^2 of 0.44–0.96 and RMSE of 31.8%–58.0% at QYZ and CBS sites, respectively (Liu et al., 2014). Similar to our results, most of those models were also found to underestimate GPP at the forest and crop sites. In Section 4.3, we also conducted the detailed comparisons with other satellite GPP products. Overall, above results illustrated that EDVI-based LUE model had the ability to estimate daily GPP estimation with a reasonable accuracy across the ChinaFLUX sites.

4.2. Model performance under different cloud cover

Since cloud change can exert noticeable effects on the daily

estimation of GPP (He et al., 2013; Wang et al., 2018), evaluating the accuracy and stability of a satellite GPP model under various cloud cover appears to be important. Thus we further validated the daily EDVI-LUE model from clear sky to cloudy sky in combination with MODIS observed cloud cover, which may be helpful for the accurate simulation of terrestrial GPP under all sky conditions.

Fig. 8 displayed the model performance from clear sky to overcast sky at a tropical evergreen broadleaf forest site (DHS) with the most frequent cloud cover (Table 1). As Frc increased from 0 to 100%, variations of daily GPP_{EDVI} were found to agree well with those of GPP_{obs} (R^2 of 0.93) (Fig. 8a). The changes in GPP_{EDVI} relative to that under clear sky were also highly consistent with those in GPP_{obs} (Fig. 8b), increasing slightly under $Frc < 30\%$ conditions and decreasing noticeably under $Frc > 40\%$ conditions (R^2 of 0.93). The overall descending trend in both GPP_{obs} and GPP_{EDVI} with the increase of Frc reflected the suppression of GPP generation caused by reduced total radiation due to clouds. More importantly, the model performed a good stability from clear sky to overcast sky (Fig. 8c,d,e,f). Overall small bias (-1.22 to $0.48 \text{ gC m}^{-2} \text{ day}^{-1}$) was found under different Frc conditions (Fig. 8c), while most of relative RMSE maintained stable magnitudes of 30% to 45% with the mean value of 43.8% (Fig. 8e). The estimated GPP_{EDVI} also had a fairly good score varying from 0.53 to 0.61 (Fig. 8f). These results indicated that the EDVI-LUE model had the capability of monitoring GPP dynamics under different cloudy sky.

On the other hand, the model was found to generate smaller bias under less Frc conditions (e.g. $Frc < 50\%$), while it more underestimated GPP_{EDVI} under overcast sky (e.g. $Frc > 70\%$) (Fig. 8a,b). The underlying reason for this could be due to the fertilization effect of diffuse radiation induced by clouds (Gu et al., 2003; Kanniah et al., 2013; Rap et al., 2015, 2018), which was not explicitly considered in current EDVI-LUE model. More diffuse radiation due to the increased Frc has been found to

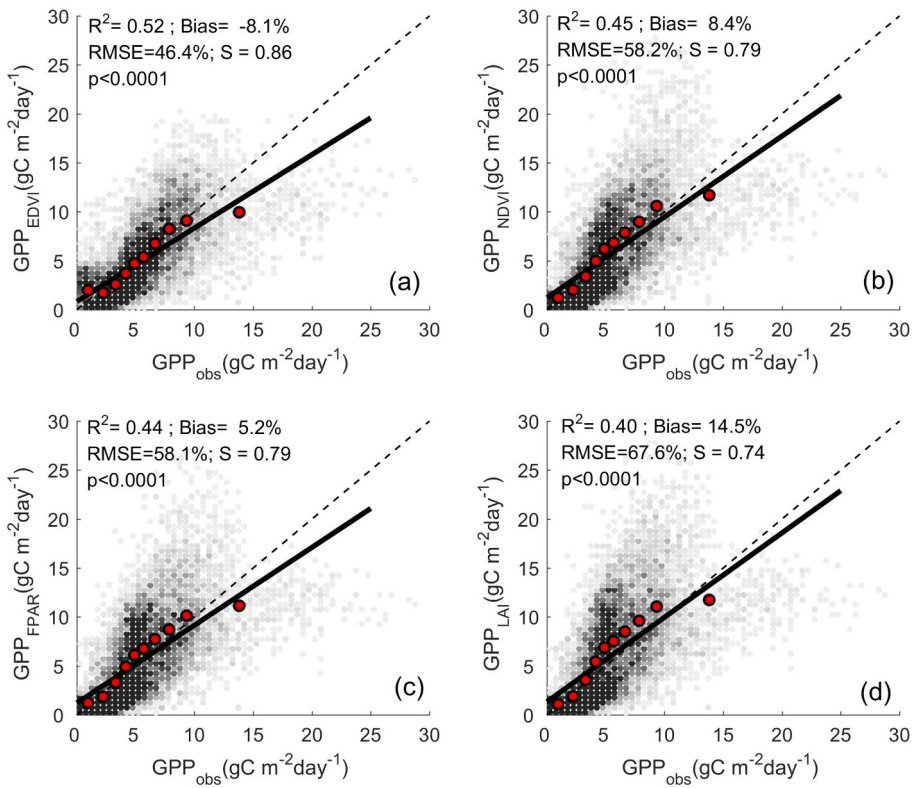


Fig. 6. Comparisons of daily GPP estimations from different FPAR schemes at all sites. Black lines are the linearly fitted lines between GPP_{obs} and GPP estimations. Red dots are the bin-averaged values. Dashed lines are 1:1 lines. (For interpretation of the references to colour in this figure legend, the reader is referred to the web version of this article.)

enhance the actual photosynthesis of those radiation-limited understory leaves (Gu et al., 2003; Knohl and Baldocchi, 2008; Li et al., 2016). In spite of such underestimation, the model displayed better R^2 and S when Frc exceeded 70% (Fig. 8d,f), implying that GPP_{EDVI} could still reflect the variation tendency in GPP_{obs} due to the change of diffuse radiation. We provided the further discussion in Section 5.2.

4.3. Comparison with satellite MOD17 and ECLUE GPP models

The daily GPP_{EDVI} were further aggregated into 8-day, monthly and yearly amount for the comparison with satellite MOD17 GPP (GPP_{MOD17}) and EC-LUE GPP (GPP_{ECLUE}) (Fig. 9). For all site estimations, three GPP models performed overall comparable accuracies at the 8-day temporal scale (Fig. 9a,d,g). GPP_{EDVI} and GPP_{ECLUE} were found to have higher R^2 (0.59 and 0.55) and smaller RMSE (40.5% and 33.2%) than GPP_{MOD17} (R^2 of 0.23 and RMSE of 44.3%). 8-day GPP_{EDVI} generated the best S of 0.88 across the sites (Fig. 9a), while GPP_{MOD17} had the lowest accuracy among the models (Fig. 9d). Although three models were found to underestimate the overall GPP for all site estimations (Fig. 9a,d,g), GPP_{EDVI} showed a relatively lower bias (-6.3%) than GPP_{MOD17} (-12.2%) and GPP_{ECLUE} (-8.8%), respectively.

Three models performed overall better accuracies at the monthly and yearly scales. Compared to 8-day estimations, GPP_{MOD17} and GPP_{ECLUE} were found to have better R^2 and higher S for monthly and yearly estimations (Fig. 9e,f; Fig. 9h,i), while their bias and RMSE changed little. By comparison, validation accuracy of GPP_{EDVI} was found to be improved significantly at the longer temporal scales (Fig. 9b, c), as indicated by R^2 increasing to 0.67 and 0.85 and S increasing to 0.85 and 0.94, respectively. RMSE of monthly and yearly GPP_{EDVI} were also noticeably reduced by 5.5% and 25.5%, respectively, when compared to the result at 8-day scale, suggesting a smaller uncertainty in the model at a longer temporal scale. Overall, the intercomparison of the satellite models illustrated the validity of EDVI-LUE model for estimating GPP at

different temporal scales.

Furthermore, the accuracies of GPP_{EDVI} , GPP_{MOD17} and GPP_{ECLUE} were found to be variable at different sites (Fig. 10). At south BNS and DHS (EBF type), although three GPP agreed well on seasonal variations and amplitudes of GPP_{obs} (Fig. 10a,b), a noticeable overestimation for GPP_{MOD17} (bias of 19.3% to 50.1%) and for GPP_{ECLUE} (bias of 15.3% to 21.5%) was found. Most of overestimation of GPP_{MOD17} and GPP_{ECLUE} was further found during the period of forest emergence and senescence (October–February) at the two sites, while GPP_{EDVI} did not show such phenomenon (Fig. 10a, b).

The forests at southeast QYZ (ENF type) and at northeast CBS (MF type) showed a stronger seasonal variation in GPP_{obs} than those at BNS and DHS. Three models generated overall best R^2 and S at the two sites than other sites (Fig. 10c,d). Differently, it was found that the peaks of 8-day GPP_{MOD17} and GPP_{ECLUE} were underestimated noticeably during middle growing seasons, leading to the total negative bias throughout the seasons. In particular, during the day of a year from 161 to 241, GPP_{MOD17} and GPP_{ECLUE} were underestimated by 26.3%–38% (or 15.1 to 21.5 $gC\ m^{-2}\ day^{-1}$) and by 15%–39.3% (or 8.6 to 24.8 $gC\ m^{-2}\ day^{-1}$) at QYZ, respectively. This could be more notable for GPP_{MOD17} (by 12.8 to 25.9 $gC\ m^{-2}\ day^{-1}$) at CBS. In contrast, the peak of GPP_{EDVI} was found to be slightly overestimated (by 2.6 to 20.7 $gC\ m^{-2}\ day^{-1}$) at QYZ and to perform closer to that of GPP_{obs} at CBS (Fig. 10c,d).

At grass sites (Fig. 10e,f), the accuracy of GPP_{EDVI} was found to be comparable with those of GPP_{MOD17} and GPP_{ECLUE} at QHB, while GPP_{EDVI} was more overestimated (bias of 9.63 $gC\ m^{-2}\ day^{-1}$) than the other two at the north NMG. At YCS site (crop type), validation showed that all satellite models severely underestimated GPP during whole growing seasons (Fig. 10g), with the bias of -20.91 $gC\ m^{-2}\ day^{-1}$ (-29.8%) for GPP_{EDVI} , -46.9 $gC\ m^{-2}\ day^{-1}$ (-66.8%) for GPP_{MOD17} and -41.8 $gC\ m^{-2}\ day^{-1}$ (-59.5%) for GPP_{ECLUE} , respectively. Although GPP_{EDVI} performed overall larger magnitudes (or smaller bias) and higher score, it had a lower R^2 and larger RMSE. This results implied

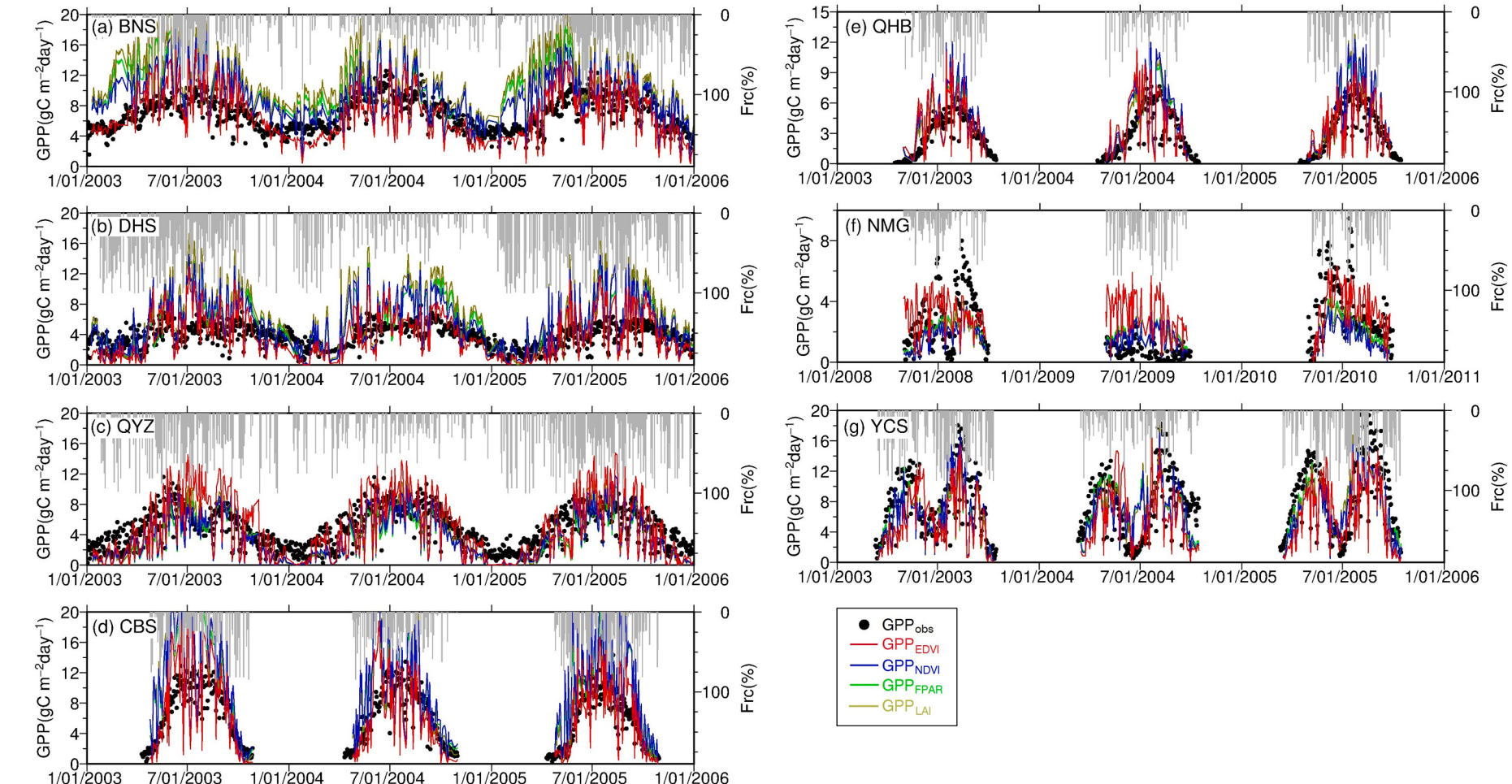


Fig. 7. Time series of daily in-situ GPP (GPP_{obs} , black dots), EDVI-based GPP (GPP_{EDVI} , red curves), NDVI-based GPP (GPP_{NDVI} , blue curves), MODIS FPAR-based GPP (GPP_{FPAR} , green curves), LAI-based GPP (GPP_{LAI} , yellow curves) under all sky. Cloud cover fraction (Frc, gray bars) is overlapped. (For interpretation of the references to colour in this figure legend, the reader is referred to the web version of this article.)

Table 3
Statistical comparison of daily GPP estimation using different FPAR schemes at the sites.

Site	Bias (%)	RMSE (%)						R ²						S		
		GPP _{EDVI}	GPP _{nEDVI}	GPP _{FPAR}	GPP _{LAI}	GPP _{EDVI}										
BNS	0.20 (3.03%)	2.55 (37.8%)	2.88 (42.7%)	4.06 (60.2%)	2.56 (37.9%)	2.95 (43.7%)	3.30 (48.8%)	3.68 (54.6%)	0.43 (2.6%)	0.26 (0.5%)	0.15 (0.5%)	0.17 (0.5%)	0.67 (0.6%)	0.62 (0.5%)	0.56 (0.5%)	
DHS	-0.16 (-4.0%)	1.54 (38.0%)	1.20 (29.6%)	2.23 (54.9%)	1.76 (43.4%)	2.23 (54.9%)	2.24 (55.2%)	2.61 (64.3%)	0.57 (2.4%)	0.56 (0.5%)	0.58 (0.5%)	0.58 (0.5%)	0.45 (0.4%)	0.46 (0.4%)	0.36 (0.3%)	
QYZ	-0.28 (-5.29%)	-1.58 (-29.8%)	-1.89 (-35.6%)	-1.53 (-28.9%)	-1.53 (38.9%)	2.07 (27.7%)	1.47 (27.0%)	1.61 (30.5%)	0.73 (4.4%)	0.74 (0.5%)	0.75 (0.5%)	0.74 (0.5%)	0.88 (0.8%)	0.91 (0.8%)	0.85 (0.8%)	
CBS	-0.31 (-4.34%)	3.38 (46.7%)	2.48 (34.3%)	2.94 (40.6%)	3.01 (42.6%)	4.77 (65.9%)	4.40 (60.7%)	4.69 (64.7%)	0.65 (2.0%)	0.52 (0.5%)	0.56 (0.5%)	0.78 (0.7%)	0.59 (0.5%)	0.63 (0.6%)	0.58 (0.58%)	
QHB	-0.90 (-17.1%)	-0.13 (-2.43%)	-0.55 (-10.5%)	-0.38 (-7.28%)	-0.38 (38.7%)	2.03 (43.0%)	2.26 (39.4%)	2.14 (40.8%)	0.49 (2.0%)	0.60 (0.6%)	0.61 (0.6%)	0.63 (0.6%)	0.84 (0.8%)	0.84 (0.8%)	0.81 (0.81%)	
NMG	0.92 (45.7%)	-0.86 (-42.5%)	-0.73 (-36.2%)	-0.87 (-43.0%)	-0.87 (58.9%)	1.19 (57.28%)	0.60 (29.8%)	0.56 (27.8%)	0.07 (0.8%)	0.22 (0.2%)	0.23 (0.2%)	0.24 (0.2%)	0.51 (0.5%)	0.26 (0.26%)	0.29 (0.29%)	
YCS	-2.89 (-31.0%)	-2.41 (-25.8%)	-2.47 (-26.5%)	-2.58 (-27.6%)	-2.58 (34.3%)	2.77 (29.6%)	2.63 (28.1%)	2.70 (28.9%)	0.42 (0.8%)	0.52 (0.5%)	0.53 (0.5%)	0.71 (0.7%)	0.73 (0.7%)	0.69 (0.7%)	0.73 (0.73%)	

that there existed a larger uncertainty in current satellite GPP models over crop systems, leading to the underperformances. This could be related to more complex biophysical constraints on the actual GPP of crop ecosystem (Schaefer et al., 2012; Yuan et al., 2014).

5. Discussions

5.1. Sensitivities of EDVI-based GPP to environmental and biophysical factors

EDVI-based EF_{veg} (EDVI-EF) indicates the available energy partitioned into plant transpiration, reflecting water loss from plant to surrounding atmosphere (Yuan et al., 2007, 2010). This process strongly correlates with canopy development in growing seasons. For example, a strong positive relationship was found between daily EDVI-EF and in-situ GPP_{obs} (R^2 of 0.87–0.97) under all sky conditions across the sites (Fig. 11). The growth of GPP_{obs} was accompanied by the increase of EDVI-EF (from around 0 to larger than 0.8), suggesting the general moisture stress during whole growing seasons. The photosynthetic activity is more limited by water availability when EDVI-EF is low, because less energy can be used for transpired water and carbon uptake. With the increase of EDVI-EF (e.g. EDVI-EF > 0.6), more available energy associated with larger water availability can be partitioned into latent heat, leading to stronger water exchange between ecosystem and atmosphere (Fig. 4). Plant photosynthesis is thus less water stressed and generates higher LUE and larger carbon uptake, particularly when receiving abundant water supply from precipitation and soil moisture in middle growing seasons.

Correlation analysis showed that environmental and biophysical factors played various roles in daily GPP_{EDVI} estimation (Fig. 12). Since radiation is the most important energy driver for EDVI-LUE model, the estimated GPP_{EDVI} was strongly related to SW_{in} (R of 0.66 to 0.79) across all sites (Fig. 12a,b,c). The correlation was found to be higher at forest sites, suggesting a stronger effect of radiation on forest GPP. Cloud change had a weak negative correlation with GPP_{EDVI} ($R < -0.21$) mainly due to the reduced radiation by increased Frc ($R < -0.41$). Environmental Ta affects the stomata activity in photosynthesis. Suited Ta would stimulate photosynthetic rate and result in larger LUE, while high Ta would induce the closure of stomata and low Ta would reduce the enzyme activity. Thus GPP_{EDVI} had a good positive relationship with Ta across all sites (Fig. 12d).

As the proxy of canopy-scale FPAR, larger nEDVI reflects a greater biomass which absorbs more PAR for the generation of GPP in growing seasons. Consequently, a noticeable positive correlation between nEDVI and GPP_{EDVI} (R of 0.37 to 0.75) was found across all vegetation types. By comparison, the correlation was higher at forest and crop sites (Fig. 12a, c) than grass sites (Fig. 12b). This may be due to the stronger correlation between GPP variation and water availability for water-limited grass than plant phenology indicated by nEDVI. It was found that water stress indicated by EDVI-EF exerted a larger effect on daily GPP_{EDVI} than nEDVI and Ta at grass sites (Fig. 12b). By comparison, the variation in GPP_{EDVI} was found to be more sensitive to nEDVI (R of 0.67 to 0.75) and to SW_{in} (R of 0.66 to 0.79) than EDVI-EF at the forests and crop sites (Fig. 12a,c). The results suggested that EDVI-based water stress was a critical controlling factor in the EDVI-LUE model. The estimated GPP_{EDVI} more correlated with water stress at the north grass sites limited by water availability due to less precipitation in arid and semiarid climate (Table 1).

5.2. Uncertainties analysis

Above results have illustrated the validity of EDVI-LUE model for the GPP estimation when validated against in-situ GPP and other satellite GPP models. However, it should be also notified that the current daily EDVI-LUE model likely underestimated GPP to a varying extent at the sites (Table 3; Fig. 9). This performance can be attributed to some

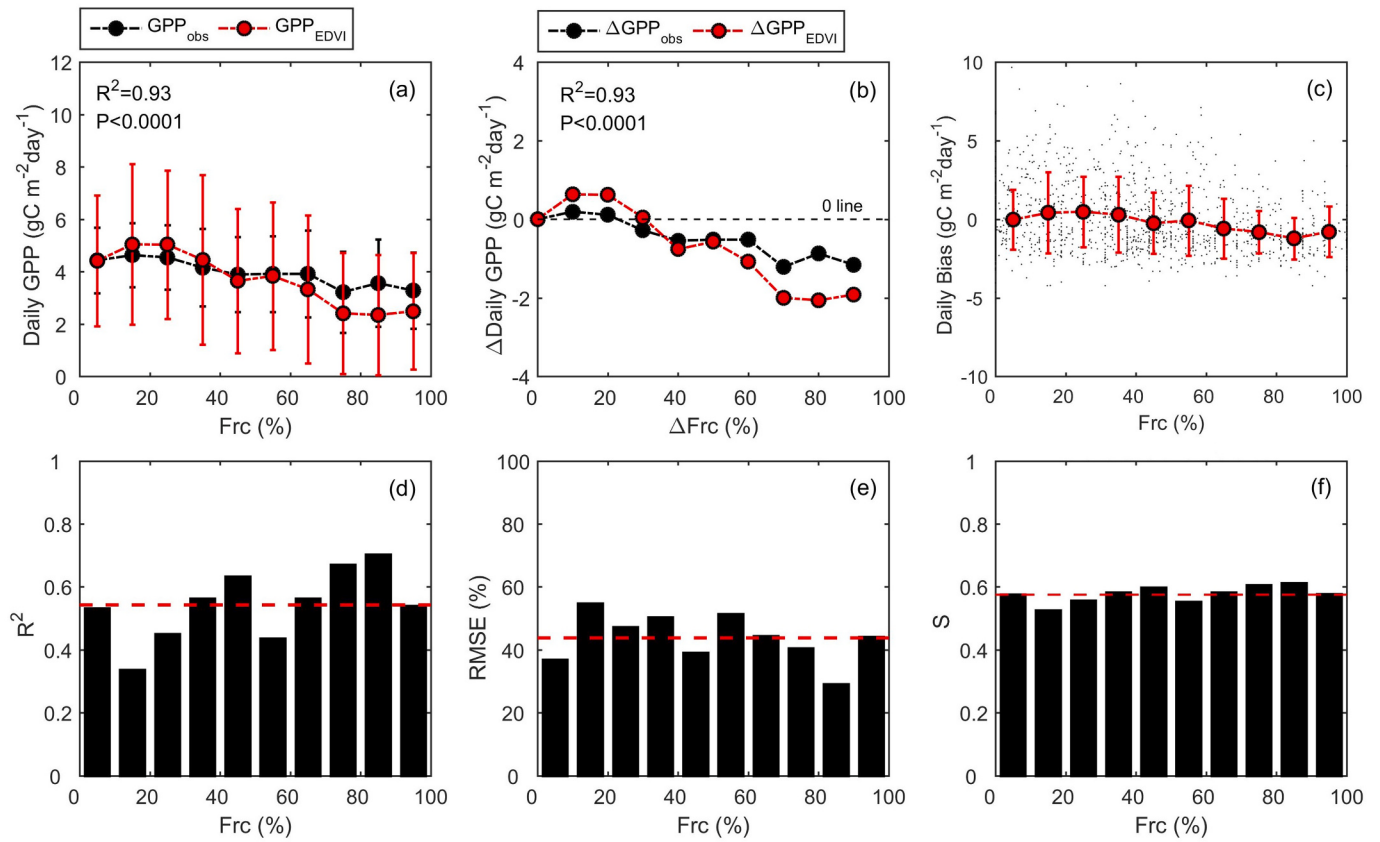


Fig. 8. Variations of (a) daily GPP_{obs} and GPP_{cal} , (b) relative changes (Δ) of daily GPP_{obs} and GPP_{cal} compared to clear sky, (c) daily bias (GPP_{EDVI} minus GPP_{obs}), (d) R^2 , (e) relative RMSE and (f) Taylor score as the function of Frc at the tropical DHS forest site. Solid circles with error bars indicate mean values with standard deviations in each bin of Frc (10%). Red Dashed lines stand for mean values for all sky. (For interpretation of the references to colour in this figure legend, the reader is referred to the web version of this article.)

uncertainties which are related to the satellite-retrieved EDVI and inaccurate parameter schemes.

5.2.1. Uncertainties from EDVI

The first issue of the microwave implement in GPP estimation is the coarse spatial resolution (~ 20 km) when compared with optic observation (0.05° or 500 m). Different from optic observations, satellite microwave observations are sensitive to all signals from vegetation, bare soil and open waters within the coarse instantaneous field of view. Our recent study has found that the signal of EDVI from vegetation can be offset largely by that from water or bare soil, especially for the surfaces covered with more than 20% open water area or with more than 50% bare soil area (Li et al., 2020). Subsequently, the offset effect may result in lower magnitudes of satellite-retrieved EDVI. Since EDVI-based schemes play a positive role in EDVI-LUE model (Fig. 12), reduced EDVI thus leads to the underestimation of GPP estimation. Furthermore, under the coarse spatial resolution, such effect could be more serious over inhomogeneous grass and crop lands than homogeneous forest canopies with larger foliage and biomass (Li et al., 2020). In this study, larger underestimations of GPP_{EDVI} were indeed found at QHB and YCS site (Fig. 7; Table 3). Spatial downscaling of EDVI is required for the further improvement of current EDVI-based GPP model.

Canopy microwave emission is sensitive to surface wetness conditions. Original satellite retrievals of EDVI and EDVI-EF were conducted under all-weather (non-rainy) conditions which were distinguished by surface rain rate from AMSR-E instantaneous observations (Li et al., 2020). However, pre-precipitation around the satellite overpass may disturb the retrievals (Li and Min, 2013). For a heavy pre-precipitation event, as we discussed above, wet canopy surfaces result in abnormally smaller EDVI during a short period. This may introduce the

uncertainty to the indication of EDVI for the day-to-day variation of vegetation moisture status and water stress at the synoptic scale. In particular, crop lands typically have high soil moisture due to precipitation or irrigation. It has been found that EDVI was able to well capture the temporal variation in crop type, but often with an underestimated magnitude (Li et al., 2020). This partly explained the performance of EDVI-LUE model at YCS site with noticeable negative bias but moderate R^2 and S (Table 3; Fig. 7g; Fig. 10g).

In contrast, satellite optic observations are more sensitive to the change of vegetation chlorophyll and greenness within a satellite footprint. The characteristic makes optic-based GPP estimations (e.g. $\text{GPP}_{\text{MOD17}}$ and $\text{GPP}_{\text{ECLUE}}$) generate less scattering (i.e. smaller RMSE) (Fig. 10).

5.2.2. Uncertainties from the maximum LUE

Determining LUE_{max} (in unit of $\text{gC m}^{-2} \text{MJ}^{-1} \text{APAR}$) is a large uncertainty source for accurately estimating the magnitude of GPP (Madani et al., 2014). In this study, we adopted the optimum LUE_{max} from Wang et al. (2015) at the same sites (Table 2). One of advantage is that they optimized LUE_{max} at each site using evolution algorithm under the effect of diffuse radiation. However, large differences in LUE_{max} exist among current GPP models. For example, LUE_{max} was set to be 2.14 for all vegetation types in EC-LUE GPP model (Yuan et al., 2007), while the value of 0.389 was used in CASA NPP model (Potter et al., 1993). In terms of GPP estimation of forests, LUE_{max} of different forest types ranged from 0.962 to 1.268 in global MOD17 GPP model (Running and Zhao, 2019), while it was 2.484 in VPM GPP model used for tropical evergreen forests (Xiao et al., 2004a). In contrast, LUE_{max} used in our study varied from 2.087 to 3.867 for forest types, which were much larger than those of MOD17 model.

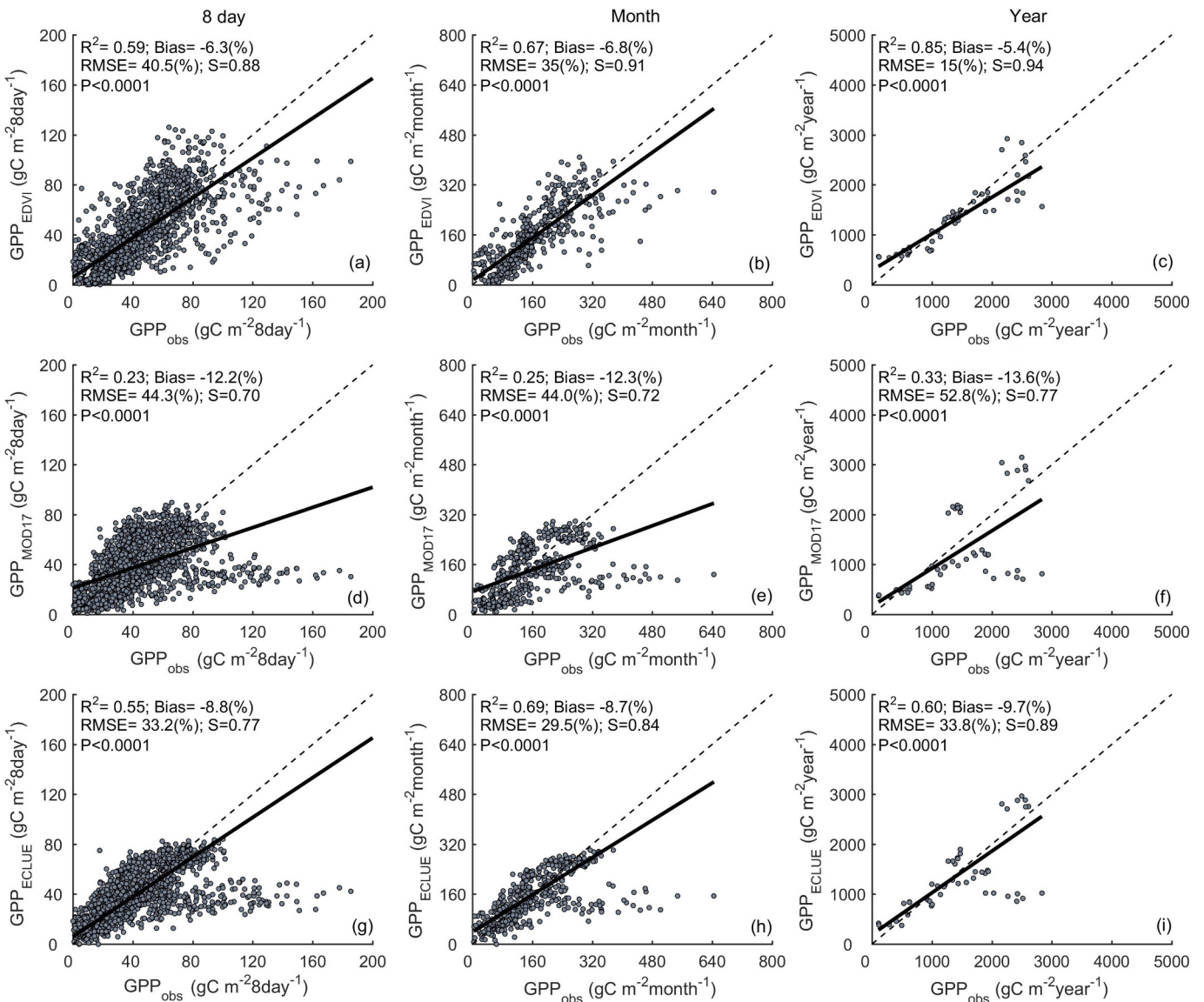


Fig. 9. Comparisons of GPP_{EDVI} (first row), GPP_{MOD} (second row) and GPP_{ECLUE} (third row) at 8-day, monthly and yearly time scales for all site estimations. Dashed lines are 1:1 lines. Solid lines are linearly-fitted lines.

In particular, LUE_{max} of crop is significantly variable among crop types (e.g. C3 and C4 types) (Yuan et al., 2015). Generally, since C4 crop (e.g. maize) has a higher photosynthetic capacity than C3 crop (e.g. wheat) under a similar climate condition, the former tends to have a larger LUE_{max} than the latter. Chen et al. (2011) have found that LUE_{max} of croplands could range widely from 0.65 to 2.0 gC m⁻² MJ⁻¹ PAR. In this study, YCS crop site contains winter wheat (C3) and summer maize (C4). All satellite LUE models significantly underestimated the growth peaks and magnitudes of GPP at the site, especially during the growth period of summer maize (Fig. 10g). Such underperformances can be largely attributed to the determination of LUE_{max}. For example, MOD17 LUE model had a smaller LUE_{max} (1.044) than EDVI-LUE (2.453) and EC-LUE model (2.14) for crop. This explained the larger underestimation (-66.8%) in GPP_{MOD17} than that in GPP_{EDVI} (-29.8%) and in GPP_{ECLUE} (-59.5%) at YCS (Fig. 10g). A separate treatment of LUE_{max} for C3 and C4 crop types based on the finer biotype-specific products can be helpful for the better modeling GPP over crop ecosystems (Yuan et al., 2015; Yan et al., 2015).

5.2.3. Uncertainties from the effect of diffuse radiation

Currently, EDVI-LUE model does not directly incorporate the scheme

of diffuse radiation. The increase of diffuse radiation due to clouds and aerosols has been found to enhance the GPP in terrestrial ecosystems (Gu et al., 2002, 2003; Alton et al., 2007a, 2007b; Knoll and Baldocchi, 2008; Zhou et al., 2021). At a canopy scale, upper canopy can reach the light saturation under intense solar radiation, while deeper canopy limited by radiation tends to increase the photosynthesis and thereby LUE via absorbing the diffused radiation (Knoll and Baldocchi, 2008; Kanniah et al., 2013; Li et al., 2016; Xin et al., 2016; Rap et al., 2015, 2018). As a result, a whole canopy may have larger LUE accompanied by reduced solar radiation (or PAR) as clouds increase, which could result in a non-linear response of GPP to clouds. Such phenomenon was found in our results (Fig. 8a,b). Compared to GPP_{obs} under clear sky (Fig. 8b), GPP_{obs} displayed a slight enhancement under mild increase of Frc (<30%), but a noticeable reduction after Frc exceeding 50%. The trend was captured by GPP_{EDVI} from our EDVI-LUE model (Fig. 8b), which was mainly attributed to the inner correlation between Frc and PAR, the use of nEDVI as an indicator of canopy development, as well as the LUE_{max} considering the diffuse radiation in Wang et al. (2015). The result also suggested that EDVI-LUE model might reflect the response of GPP to the total intercepted light at the canopy or ecosystem scale, although the current model did not explicitly incorporate the effect of diffuse

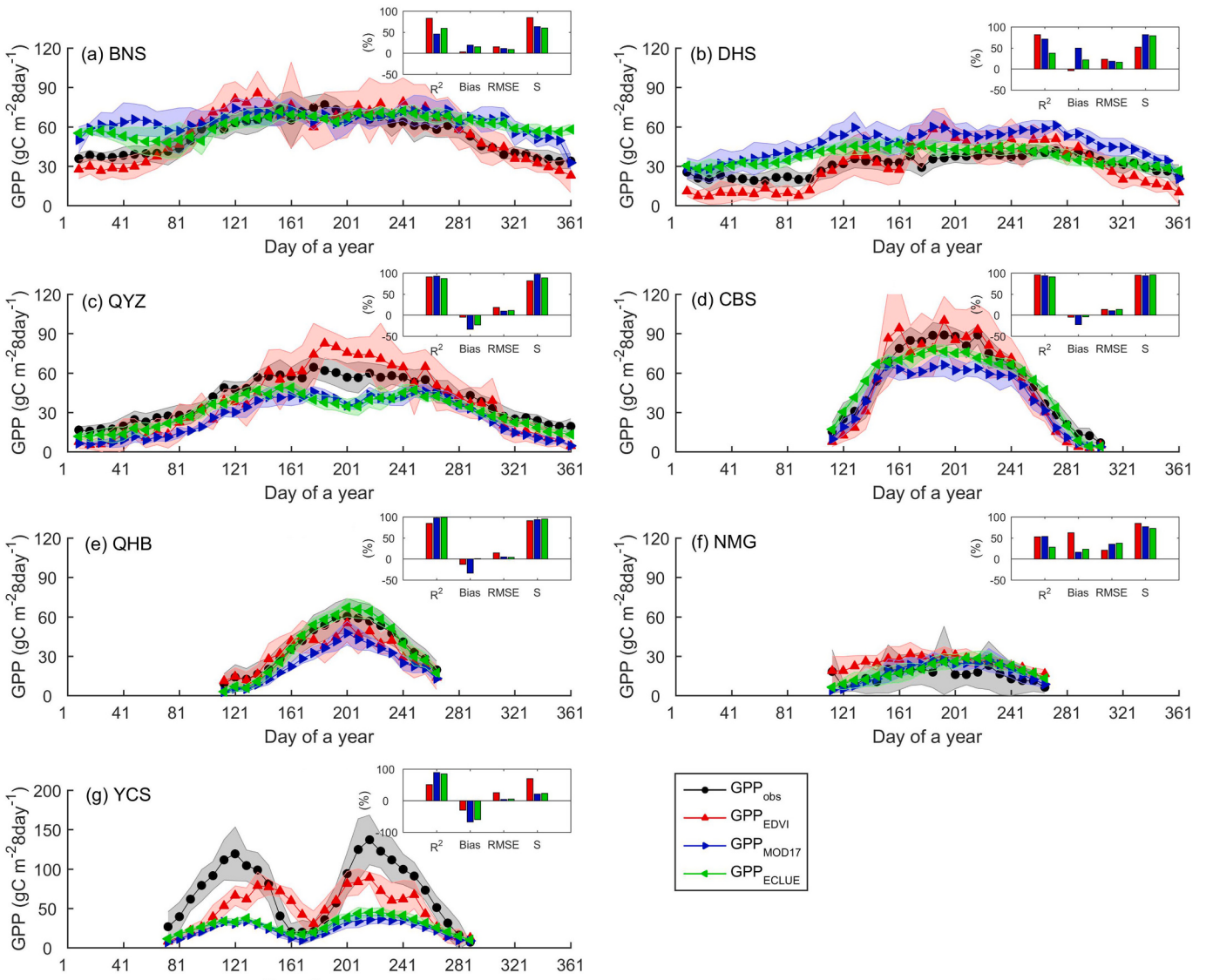


Fig. 10. Seasonal variations of 8-day GPP_{obs} (black), GPP_{EDVI} (red), GPP_{MOD17} (blue) and GPP_{ECLUE} (green) at the multiple-year average scale. The shadows stand for mean \pm standard deviation. Statistical comparisons at each site were shown in the bar plots, including R², relative bias, relative RMSE and Taylor score. (For interpretation of the references to colour in this figure legend, the reader is referred to the web version of this article.)

radiation.

In spite of this, the consideration of diffuse radiation in our current model remained insufficient, especially under heavy cloud cover conditions. For example, we noticed that the estimated daily GPP_{EDVI} at middle latitude sites (e.g. CBS, QHB, NMG and YCS, Fig. 7) showed some noticeable underestimations under larger cloud cover conditions. It was also confirmed at south DHS forest site for Frc > 60% (Fig. 8a,b). Similarly, both of satellite MOD17 and EC-LUE models ignored the schemes of diffuse radiation and had large underestimations (Fig. 10). Some satellite GPP models have been found to consider the effect of diffuse radiation (Wang et al., 2015; Yan et al., 2017; Wang et al., 2018). For example, Wang et al. (2015) took diffused conditions into MOD17 LUE model and generated more accurate GPP estimation with higher amplitudes during the peak seasons at CBS and YCS site. Wang et al. (2018) used cloudiness index to estimate diffuse radiation ratio and incorporated it into GPP and ET model at a high-latitude forest. In this direction, the further improvement of EDVI-LUE model can benefit from the incorporation of diffuse radiation scheme.

6. Conclusions

This study developed a new light use efficiency (LUE) GPP model coupled with satellite passive microwave measurements for daily GPP estimations under all sky. Microwave vegetation index EDVI and EDVI-derived variables are primary forcing variables in the model. The normalized EDVI (nEDVI) indicating canopy-scale leaf development was used as a proxy of FPAR. The nEDVI-based FPAR was found to well correlate with in-situ GPP (GPP_{obs}) at daily scale. Compared to FPAR schemes based on optic observations (e.g. NDVI, LAI and MODIS FPAR), the nEDVI-based FPAR showed a less saturation and higher correlation with daily GPP_{obs} under more cloud cover. EDVI-derived evaporative fraction of vegetation (EDVI-EF) was used to quantify the daily water stress of LUE and showed a strong correlation with GPP_{obs}.

Seven flux tower sites of ChinaFLUX network with long-term (2003–2010) measurements were used to validate the EDVI-based LUE (EDVI-LUE) model. Results showed that estimated GPP (GPP_{EDVI}) performed an overall reasonable accuracy (bias of $-0.47 \text{ gC m}^{-2} \text{ day}^{-1}$ or -8.1% , Taylor score of 0.86) at the daily scale across the sites. Overall better bias, R² and comprehensive skill score for GPP_{EDVI} were

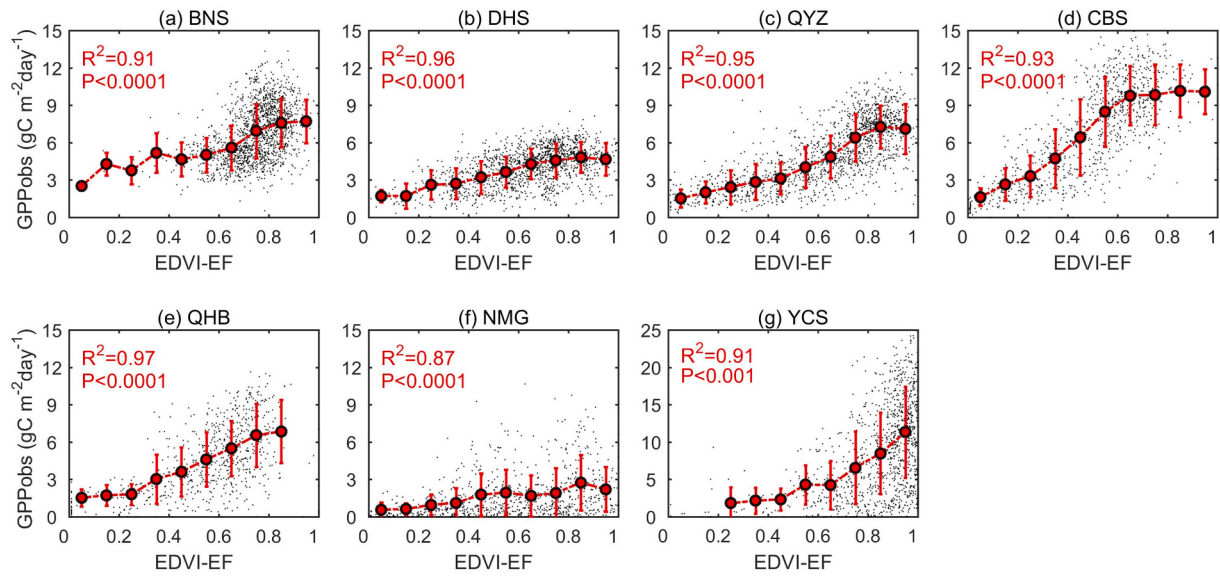


Fig. 11. Relationship between daily GPP_{obs} and EDVI-EF across the sites. Red spots are averaged values in each bin of 0.1. Error bars represent standard deviation. Statistic results are based on the bin-averaged values. (For interpretation of the references to colour in this figure legend, the reader is referred to the web version of this article.)

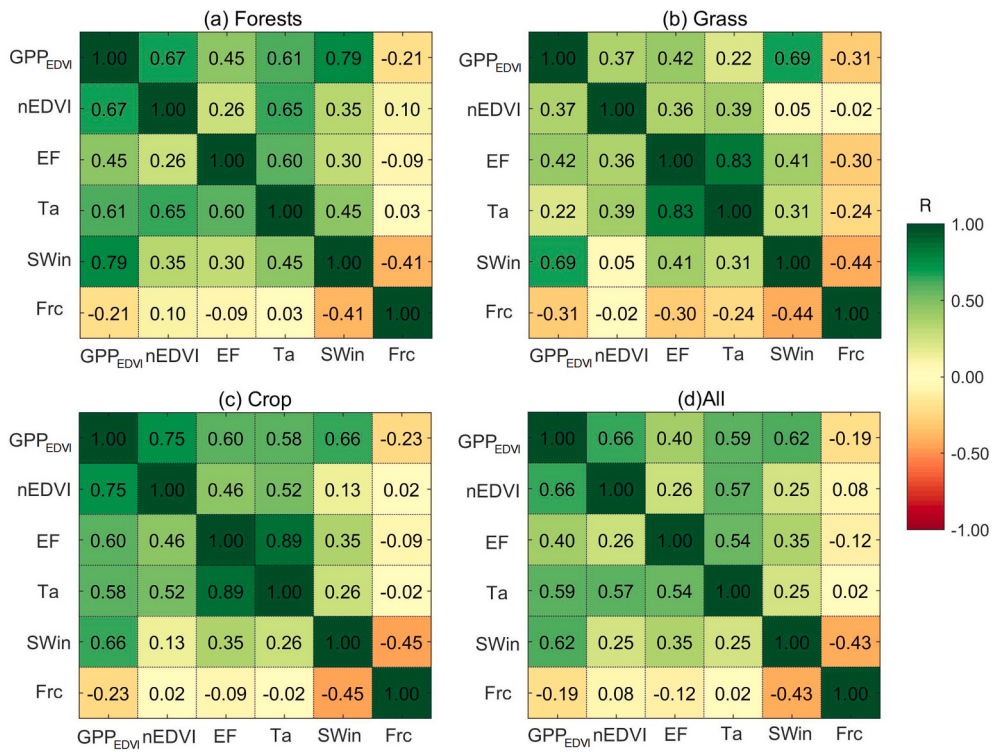


Fig. 12. Correlation matrixes between daily GPP_{EDVI} and the factors in EDVI-LUE model at different vegetation type sites.

found at forest sites than at grass and crop sites. EDVI-LUE model was able to well capture the variations in GPP_{obs} with stable accuracies from clear sky to cloudy sky (bias of -1.22 to $0.48 \text{ gC m}^{-2} \text{ day}^{-1}$, skill score of 0.53 to 0.61), while the larger underestimation of GPP_{EDVI} was found under more cloudy sky (cloud cover $>50\%$).

Further comparisons with satellite optic MOD17 GPP (GPP_{MOD17} , Zhao et al., 2005) and EC-LUE GPP (GPP_{ECLUE} , Yuan et al., 2007, 2010) showed that GPP_{EDVI} performed overall better accuracy for all site estimations from 8-day to yearly scales. Particularly, bias for GPP_{EDVI} was found to be significantly smaller than those for GPP_{MOD17} and GPP_{ECLUE}

across forest sites, while the latter two were more overestimated at evergreen broadleaf forests. GPP_{EDVI} showed larger errors at grass sites. All three satellite LUE models seriously underestimated the growth peak and amount of GPP at crop site, although EDVI-LUE performed relatively smaller negative bias. These results indicated that current EDVI-LUE model had a better capability of estimating daily GPP over forests, while over grass and crop lands, it might suffer a larger uncertainty which is related to the coarse spatial resolution, surface wetness and heavy pre-precipitation events.

In summary, this study is the first attempt toward the integration of

microwave-derived variables into LUE model for daily GPP estimation. The proposed model has a potential of being used for mapping spatio-temporally continuous daily GPP under various clouds when further coupled with satellite radiation observations and reanalysis data, such as all-sky surface radiation from Clouds and the Earth's Radiant Energy System (CERES) and meteorological reanalysis from ERA5. In order to retrieve more accurate GPP under cloudy sky, future improvements of the model will include the effect of direct and diffuse radiation as well as atmospheric CO₂ concentration on photosynthesis. Finally, this microwave-based method may have difficulties in estimating ecosystem GPP at a small scale. The spatial downscaling of EDVI and EDVI-EF is underway.

Declaration of Competing Interest

The authors declare that they have no known competing financial interests or personal relationships that could have appeared to influence the work reported in this paper.

Acknowledgments

The authors would like to thank the three anonymous reviewers for their valuable comments which have helped us greatly improve the manuscript. This work was supported by the National Key Research and Development Program of China (Grant No. 2017YFC1501402), the National Natural Science Foundation of China NSFC (Grant No. 41675022, 41661144007, 41830104, 42105123), the Fundamental Research Funds for the Central Universities (Grant No. WK20280000138), and the Jiangsu Provincial 2011 Program (Collaborative Innovation Center of Climate Change).

References

- Alton, P.B., North, P.R., Los, S.O., 2007a. The impact of diffuse sunlight on canopy light-use efficiency, gross photosynthetic product and net ecosystem exchange in three forest biomes. *Glob. Chang. Biol.* 13 (4), 776–787.
- Alton, P.B., Ellis, R., Los, S.O., North, P.R., 2007b. Improved global simulations of gross primary product based on a separate and explicit treatment of diffuse and direct sunlight. *J. Geophys. Res.* 112.
- Anav, A., Friedlingstein, P., Beer, C., Ciais, P., Harper, A., Jones, C., Peylin, P., 2015. Spatiotemporal patterns of terrestrial gross primary production: a review. *Rev. Geophys.* 53 (3), 785–818.
- Becker, F., Choudhury, B.J., 1988. Relative sensitivity of Normalized Difference Vegetation Index (NDVI) and Microwave Polarization Difference Index (MPDI) for vegetation and desertification monitoring. *Remote Sens. Environ.* 24 (2), 297–311.
- Beer, C., Reichstein, M., Tomelleri, E., Ciais, P., Jung, M., Carvalhais, N., Bonan, G.B., 2010. Terrestrial gross carbon dioxide uptake: global distribution and covariation with climate. *Science* 329 (5993), 834–838.
- Berry, Z.C., Johnson, D.M., Reinhardt, K., 2015. Vegetation-zonation patterns across a temperate mountain cloud forest ecotone are not explained by variation in hydraulic functioning or water relations. *Tree Physiol.* 35 (9), 925–935.
- Chen, T., van der Werf, G.R., Dolman, A.J., Groenendijk, M., 2011. Evaluation of cropland maximum light use efficiency using eddy flux measurements in North America and Europe. *Geophys. Res. Lett.* 38 (14).
- Cornic, G., 2000. Drought stress inhibits photosynthesis by decreasing stomatal aperture – not by affecting ATP synthesis. *Trends Plant Sci.* 5 (5), 187–188.
- Cox, P., Jones, C., 2008. Illuminating the modern dance of climate and CO₂. *Science* 321, 1642–1644.
- Damm, A., Paul-Limoges, E., Haghghi, E., Simmer, C., Morsdorf, F., Schneider, F.D., Rascher, U., 2018. Remote sensing of plant-water relations: an overview and future perspectives. *J. Plant Physiol.* 227, 3–19.
- Flexas, J., Medrano, H., 2002. Drought-inhibition of photosynthesis in C3 plants: stomatal and non-stomatal limitations revisited. *Ann. Bot.* 89 (2), 183–189.
- Gu, L., Baldocchi, D., Verma, S.B., Black, T.A., Vesala, T., Falge, E.M., Dowty, P.R., 2002. Advantages of diffuse radiation for terrestrial ecosystem productivity. *J. Geophys. Res.* 107, 4050.
- Gu, L., Baldocchi, D.D., Wofsy, S.C., Munger, J.W., Michalsky, J.J., Urbanski, S.P., Boden, T.A., 2003. Response of a deciduous forest to the Mount Pinatubo eruption: enhanced photosynthesis. *Science* 299 (5615), 2035–2038.
- Gu, X., Wang, L., Su, X., Yi, X., Chen, X., Yao, R., Wang, S., 2021. Environmental factors modulate the diffuse fertilization effect on gross primary productivity across Chinese ecosystems. *Sci. Total Environ.* 793, 148443.
- He, M., Ju, W., Zhou, Y., Chen, J., He, H., Wang, S., Li, Y., 2013. Development of a two-leaf light use efficiency model for improving the calculation of terrestrial gross primary productivity. *Agric. For. Meteorol.* 173, 28–39.
- Janssens, I.A., Freibauer, A., Ciais, P., Smith, P., Nabuurs, G.-J., Folberth, G., Schulze, E.D., 2003. Europe's terrestrial biosphere absorbs 7 to 12% of European anthropogenic CO₂ emissions. *Science* 300 (5625), 1538–1542.
- Jarvis, P.G., 1976. The interpretation of the variations in leaf water potential and stomatal conductance found in canopies in the field. *Philos. Trans. R. Soc. B* 273 (927), 593–610.
- Jones, H.G., 1998. Stomatal control of photosynthesis and transpiration. *J. Exp. Bot.* 49 (90001), 387–398.
- Kanniah, K.D., Beringer, J., Hutley, L.B., 2013. Exploring the link between clouds, radiation, and canopy productivity of tropical savannas. *Agric. For. Meteorol.* 182, 304–313.
- Kelliher, F.M., Leuning, R., Raupach, M., Schulze, E.-D., 1995. Maximum conductances for evaporation from global vegetation types. *Agric. For. Meteorol.* 73, 1–16.
- Knapp, A.K., Smith, W.K., 1987. Stomatal and photosynthetic responses during sun/shade transitions in subalpine plants: influence on water use efficiency. *Oecologia* 74 (1), 62–67.
- Knapp, A.K., Smith, W.K., 1988. Effect of water stress on stomatal and photosynthetic responses in subalpine plants to cloud patterns. *Am. J. Bot.* 75 (6), 851–858.
- Knohl, A., Baldocchi, D.D., 2008. Effects of diffuse radiation on canopy gas exchange processes in a forest ecosystem. *J. Geophys. Res.* 113.
- Konings, A.G., Rao, K., Steele-Dunne, Susan C., 2019. Macro to micro: microwave remote sensing of plant water content for physiology and ecology. *New Phytol.* 223 (3).
- Kottek, M., Grieser, J., Beck, C., Rudolf, B., Rubel, F., 2006. World map of the Köppen-Geiger climate classification updated. *Meteorol. Z.* 15 (3), 259–263.
- Li, R., Min, Q., 2013. Dynamic response of microwave land surface properties to precipitation in Amazon rainforest. *Remote Sens. Environ.* 133, 183–192.
- Li, R., Min, Q., Lin, B., 2009. Estimation of evapotranspiration in a mid-latitude forest using the Microwave Emissivity Difference Vegetation Index (EDVI). *Remote Sens. Environ.* 113 (9), 2011–2018.
- Li, T., Kromdijk, J., Heuvelink, E., van Noort, F.R., Kaiser, E., Marcelis, L.F.M., 2016. Effects of diffuse light on radiation use efficiency of two anthurium cultivars depend on the response of stomatal conductance to dynamic light intensity. *Front. Plant Sci.* 7, 56.
- Li, R., Wang, Y., Hu, J., Wang, Y., Min, Q., Bergeron, Y., Fu, Y., 2020. Spatiotemporal variations of satellite microwave emissivity difference vegetation index in China under clear and cloudy skies. *Earth Space Sci.* 7 (5).
- Liu, Z., Wang, L., Wang, S., 2014. Comparison of different GPP models in China using MODIS images and ChinaFLUX data. *Remote Sens.* 6 (10), 10215–10231.
- Liu, Y.Y., van Dijk, A.I.J.M., de Jeu, R.A.M., Canadell, J.G., McCabe, M.F., Evans, J.P., Wang, G., 2015. Recent reversal in loss of global terrestrial biomass. *Nat. Clim. Chang.* 5 (5), 470–474.
- Liu, Q., Zhang, S., Zhang, H., Bai, Y., Zhang, J., 2020. Monitoring drought using composite drought indices based on remote sensing. *Sci. Total Environ.* 711, 134585.
- Lyons, D.S., Dobrowski, S.Z., Holden, Z.A., Maneta, M.P., Sala, A., 2021. Soil moisture variation drives canopy water content dynamics across the western U.S. *Remote Sens. Environ.* 253, 112233.
- Ma, J., Yan, X., Dong, W., Chou, J., 2015. Gross primary production of global forest ecosystems has been overestimated. *Sci. Rep.* 5 (1), 10820.
- Madani, N., Kimball, J.S., Affleck, D.L.R., Katte, J., Graham, J., van Bodegom, P.M., Running, S.W., 2014. Improving ecosystem productivity modeling through spatially explicit estimation of optimal light use efficiency. *J. Geophys. Res.* 119 (9), 1755–1769.
- Min, Q., Lin, B., 2006a. Remote sensing of evapotranspiration and carbon uptake at Harvard Forest. *Remote Sens. Environ.* 100 (3), 379–387.
- Min, Q., Lin, B., 2006b. Determination of spring onset and growing season leaf development using satellite measurements. *Remote Sens. Environ.* 104 (1), 96–102.
- Min, Q., Lin, B., Li, R., 2010. Remote sensing vegetation hydrological states using passive microwave measurements. *IEEE J. Select. Topics Appl. Earth Observ. Remote Sensing* 3 (1), 124–131.
- Momen, M., Wood, J.D., Novick, K.A., Pangle, R., Pockman, W.T., McDowell, N.G., Konings, A.G., 2017. Interacting effects of leaf water potential and biomass on vegetation optical depth. *J. Geophys. Res.* 122 (11), 3031–3046.
- Monteith, J.L., 1972. Solar radiation and productivity in tropical ecosystems. *J. Appl. Ecol.* 9 (3), 747.
- Monteith, J.L., 1977. Climate and the efficiency of crop production in Britain. *Philos. Trans. R. Soc. B* 281 (980), 277–294.
- Mu, Q., Heinisch, F.A., Zhao, M., Running, S.W., 2007. Development of a global evapotranspiration algorithm based on MODIS and global meteorology data. *Remote Sens. Environ.* 111 (4), 519–536.
- Mu, Q., Zhao, M., Running, S.W., 2011. Improvements to a MODIS global terrestrial evapotranspiration algorithm. *Remote Sens. Environ.* 115 (8), 1781–1800.
- Myneni, R.B., Williams, D.L., 1994. On the relationship between FAPAR and NDVI. *Remote Sens. Environ.* 49 (3), 200–211.
- Nishida, K., Nemani, R.R., Running, S.W., Glassy, J.M., 2003. An operational remote sensing algorithm of land surface evaporation. *J. Geophys. Res.* 108, 4270.
- Paloszka, S., Pampalon, P., 1992. Microwave vegetation indexes for detecting biomass and water conditions of agricultural crops. *Remote Sens. Environ.* 40 (1), 15–26.
- Peng, Y., Gitelson, A.A., 2012. Remote estimation of gross primary productivity in soybean and maize based on total crop chlorophyll content. *Remote Sens. Environ.* 117, 440–448.
- Potter, C.S., Randerson, J.T., Field, C.B., Matson, P.A., Vitousek, P.M., Mooney, H.A., Klooster, S.A., 1993. Terrestrial ecosystem production: a process model based on global satellite and surface data. *Glob. Biogeochem. Cycles* 7 (4), 811–841.
- Rap, A., Spracklen, D.V., Mercado, L.M., Reddington, C.L., Haywood, J.M., Ellis, R., Coupe, N.R., 2015. Fires increase Amazon forest productivity through increases in diffuse radiation. *Geophys. Res. Lett.* 42 (11), 4654–4662.

- Rap, A., Scott, C.E., Reddington, C.L., Mercado, L., Ellis, R.J., Garraway, S., Hewitt, C.N., 2018. Enhanced global primary production by biogenic aerosol via diffuse radiation fertilization. *Nat. Geosci.* 11 (9), 640–644.
- Reichstein, M., Papale, D., Valentini, R., Aubinet, M., Bernhofer, C., Knohl, A., Pilegaard, K., 2007. Determinants of terrestrial ecosystem carbon balance inferred from European eddy covariance flux sites. *Geophys. Res. Lett.* 34 (1).
- Rocha, A.V., Su, H.-B., Vogel, C.S., Schmid, H.P., Curtis, P.S., 2004. Photosynthetic and water use efficiency responses to diffuse radiation by an Aspen-dominated northern hardwood Forest. *For. Sci.* 50 (6), 793.
- Rodríguez-Fernández, N.J., Mialon, A., Mermoz, S., Bouvet, A., Richaume, P., Bitar, A.A., Toan, T.L., 2018. An evaluation of SMOS L-band vegetation optical depth (L-VOD) data sets: high sensitivity of L-VOD to above-ground biomass in Africa. *Biogeosciences* 15 (14), 4627–4645.
- Ruimy, A., Kergoat, L., Bondeau, A., 1999. Comparing global models of terrestrial net primary productivity (NPP): analysis of differences in light absorption and light-use efficiency. *Glob. Chang. Biol.* 5, 56–64.
- Running, S.W., Zhao, M., 2019. User's Guide Daily GPP and Annual NPP (MOD17A2H/A3H) and Year-End GapFilled (MOD17A2HGF/A3HGF) Products NASA Earth Observing System MODIS Land Algorithm (for Collection 6). University of Montana, Missoula, MT.
- Samanta, A., Ganguly, S., Hashimoto, H., Devadiga, S., Vermote, E., Knyazikhin, Y., Myneni, R.B., 2010. Amazon forests did not green-up during the 2005 drought. *Geophys. Res. Lett.* 37 (5).
- Schaefer, K., Schwalm, C.R., Williams, C., Arain, M.A., Barr, A., Chen, J.M., Hollinger, D.Y., 2012. A model-data comparison of gross primary productivity: results from the North American Carbon Program site synthesis. *J. Geophys. Res.* 117 (3).
- Schreel, J.D.M., Steppe, K., 2019. Foliar water uptake changes the world of tree hydraulics. *Npj Climate Atmos. Sci.* 2 (1), 1–2.
- Shi, J., Jackson, T., Tao, J., Du, J., Bindlish, R., Lu, L., Chen, K.S., 2008. Microwave vegetation indices for short vegetation covers from satellite passive microwave sensor AMSR-E. *Remote Sens. Environ.* 112 (12), 4285–4300.
- Sims, D.A., Rahman, A.F., Cordova, V.D., Baldocchi, D.D., Flanagan, L.B., Goldstein, A.H., Schmid, H.P., 2005. Midday values of gross CO₂ flux and light use efficiency during satellite overpasses can be used to directly estimate eight-day mean flux. *Agric. For. Meteorol.* 131 (1), 1–12.
- Sims, D.A., Rahman, A.F., Cordova, V.D., El-Masri, B.Z., Baldocchi, D.D., Bolstad, P.V., Misson, L., 2008. A new model of gross primary productivity for North American ecosystems based solely on the enhanced vegetation index and land surface temperature from MODIS. *Remote Sens. Environ.* 112 (4), 1633–1646.
- Taylor, J.L.A., 1994. On the temperature dependence of soil respiration. *Funct. Ecol.* 8, 315–323.
- Taylor, K.E., 2001. Summarizing multiple aspects of model performance in a single diagram. *J. Geophys. Res. Atmos.* 106 (D7), 7183–7192.
- Teubner, I.E., Forkel, M., Jung, M., Liu, Y.Y., Miralles, D.G., Parinussa, R., Tramontana, G., 2018. Assessing the relationship between microwave vegetation optical depth and gross primary production. *Int. J. Appl. Earth Obs. Geoinf.* 65, 79–91.
- Teubner, I.E., Forkel, M., Camps-Valls, G., Jung, M., Miralles, D.G., Tramontana, G., Dorigo, W.A., 2019. A carbon sink-driven approach to estimate gross primary production from microwave satellite observations. *Remote Sens. Environ.* 229, 100–113.
- Thornton, P.E., 1998. Regional Ecosystem Simulation: Combining Surface- and Satellite Based Observations to Study Linkages between Terrestrial Energy and Mass Budgets. Thesis. University of Montana, p. 1015.
- Tian, F., Brandt, M., Liu, Y.Y., Verger, A., Tagesson, T., Diouf, A.A., Fensholt, R., 2016. Remote sensing of vegetation dynamics in drylands: evaluating vegetation optical depth (VOD) using AVHRR NDVI and in situ green biomass data over West African Sahel. *Remote Sens. Environ.* 177, 265–276.
- Ulaby, F.T., Sarabandi, K., McDonald, K., Whitt, M., Dobson, M.C., 1990. Michigan microwave canopy scattering model. *Int. J. Remote Sens.* 11 (7), 1223–1253.
- Velpuri, N.M., Senay, G.B., Singh, R.K., Bohms, S., Verdin, J.P., 2013. A comprehensive evaluation of two MODIS evapotranspiration products over the conterminous United States: using point and gridded FLUXNET and water balance ET. *Remote Sens. Environ.* 139, 35–49.
- Wang, K., Dickinson, R.E., 2012. A review of global terrestrial evapotranspiration: observation, modeling, climatology, and climatic variability. *Rev. Geophys.* 50 (2).
- Wang, S., Huang, K., Yan, H., Yan, L., Wang, H., Wang, Y., 2015. Improving the light use efficiency model for simulating terrestrial vegetation gross primary production by the inclusion of diffuse radiation across ecosystems in China. *Ecol. Complex.* 23, 1–13.
- Wang, S., Ibrom, A., Bauer-Gottwein, P., Garcia, M., 2018. Incorporating diffuse radiation into a light use efficiency and evapotranspiration model: an 11-year study in a high latitude deciduous forest. *Agric. For. Meteorol.* 248, 479–493.
- Wang, Y., Li, R., Min, Q., Fu, Y., Wang, Y., Zhong, L., Fu, Y., 2019a. A three-source satellite algorithm for retrieving all-sky evapotranspiration rate using combined optical and microwave vegetation index at twenty AsiaFlux sites. *Remote Sens. Environ.* 235, 111463.
- Wang, Y., Li, R., Min, Q., Zhang, L., Yu, G., Bergeron, Y., 2019b. Estimation of vegetation latent heat flux over three forest sites in ChinaFLUX using satellite microwave vegetation water content index. *Remote Sens.* 11 (11), 1359.
- Waring, R.H., Law, B.E., Goulden, M.L., Bassow, S.L., McCreight, R.W., Wofsy, S.C., Bazzaz, F.A., 1995. Scaling gross ecosystem production at Harvard Forest with remote sensing: a comparison of estimates from a constrained quantum-use efficiency model and eddy correlation. *Plant Cell Environ.* 18 (10), 1201–1213.
- Wu, C., Niu, Z., Tang, Q., Huang, W., Rivard, B., Feng, J., 2009. Remote estimation of gross primary production in wheat using chlorophyll-related vegetation indices. *Agric. For. Meteorol.* 149 (6), 1015–1021.
- Xiao, X., Hollinger, D., Aber, J., Goltz, M., Davidson, E.A., Zhang, Q., Moore, B., 2004a. Satellite-based modeling of gross primary production in an evergreen needleleaf forest. *Remote Sens. Environ.* 89 (4), 519–534.
- Xiao, X., Zhang, Q., Braswell, B., Urbanski, S., Boles, S., Wofsy, S., Ojima, D., 2004b. Modeling gross primary production of temperate deciduous broadleaf forest using satellite images and climate data. *Remote Sens. Environ.* 91 (2), 256–270.
- Xin, Q., Gong, P., Suyker, A.E., Si, Y., 2016. Effects of the partitioning of diffuse and direct solar radiation on satellite-based modeling of crop gross primary production. *Int. J. Appl. Earth Obs. Geoinf.* 50, 51–63.
- Yan, H., Wang, S., Billesbach, D., Oechel, W., Bohrer, G., Meyers, T., Rahman, F., 2015. Improved global simulations of gross primary product based on a new definition of water stress factor and a separate treatment of C3 and C4 plants. *Ecol. Model.* 297, 42–59.
- Yan, H., Wang, S.-Q., Yu, K.-L., Wang, B., Yu, Q., Bohrer, G., Shugart, H.H., 2017. A novel diffuse fraction-based two-leaf light use efficiency model: an application quantifying photosynthetic seasonality across 20 AmeriFlux flux tower sites. *J. Adv. Model. Earth Syst.* 9 (6), 2317–2332.
- Yang, D., Xu, X., Xiao, F., Xu, C., Luo, W., Tao, L., 2021. Improving modeling of ecosystem gross primary productivity through re-optimizing temperature restrictions on photosynthesis. *Sci. Total Environ.* 788, 147805.
- Yao, Y., Liang, S., Li, X., Zhang, Y., Chen, J., Jia, K., Xu, J., 2017. Estimation of high-resolution terrestrial evapotranspiration from Landsat data using a simple Taylor skill fusion method. *J. Hydrol.* 553, 508–526.
- Yu, G.-R., Wen, X.-F., Sun, X.-M., Tanner, B.D., Lee, X., Chen, J.-Y., 2006. Overview of ChinaFLUX and evaluation of its eddy covariance measurement. *Agric. For. Meteorol.* 137 (3), 125–137.
- Yu, G.-R., Zhang, L.-M., Sun, X.-M., Fu, Y.-L., Wen, X.-F., Wang, Q.-F., Liu, Y.-F., 2008. Environmental controls over carbon exchange of three forest ecosystems in eastern China. *Glob. Chang. Biol.* 14 (11), 2555–2571.
- Yuan, W., Liu, S., Zhou, G., Zhou, G., Tieszen, L.L., Baldocchi, D.D., Goulden, M.L., 2007. Deriving a light use efficiency model from eddy covariance flux data for predicting daily gross primary production across biomes. *Agric. For. Meteorol.* 143 (3), 189–207.
- Yuan, W., Liu, S., Yu, G., Bonnefond, J.-M., Chen, J., Davis, K., Rossi, F., 2010. Global estimates of evapotranspiration and gross primary production based on MODIS and global meteorology data. *Remote Sens. Environ.* 114 (7), 1416–1431.
- Yuan, W., Cai, W., Xia, J., Chen, J., Liu, S., Dong, W., Beringer, J., 2014. Global comparison of light use efficiency models for simulating terrestrial vegetation gross primary production based on the LaThuile database. *Agric. For. Meteorol.* 192, 108–120.
- Yuan, W., Cai, W., Nguy-Robertson, A.L., Fang, H., Suyker, A.E., Chen, Y., Zhang, H., 2015. Uncertainty in simulating gross primary production of cropland ecosystem from satellite-based models. *Agric. For. Meteorol.* 207, 48–57.
- Zhang, Y., Song, C., Sun, G., Band, L.E., Noormets, A., Zhang, Q., 2015. Understanding moisture stress on light use efficiency across terrestrial ecosystems based on global flux and remote-sensing data. *J. Geophys. Res.* 120 (10), 2053–2066.
- Zhang, K., Kimball, J.S., Running, S.W., 2016a. A review of remote sensing based actual evapotranspiration estimation: a review of remote sensing evapotranspiration. *Wiley Interdiscip. Rev. Water* 3 (6), 834–853.
- Zhang, Y., Xiao, X., Zhou, S., Ciais, P., McCarthy, H., Luo, Y., 2016b. Canopy and physiological controls of GPP during drought and heat wave. *Geophys. Res. Lett.* 43 (7), 3325–3333.
- Zhang, Y., Li, R., Min, Q., Bo, H., Fu, Y., Wang, Y., Gao, Z., 2019. The controlling factors of atmospheric formaldehyde (HCHO) in Amazon as seen from satellite. *Earth Space Sci.* 6 (6), 959–971.
- Zhao, M., Heinsch, F.A., Nemani, R.R., Running, S.W., 2005. Improvements of the MODIS terrestrial gross and net primary production global data set. *Remote Sens. Environ.* 95, 164–176.
- Zhou, J., Jia, L., Menenti, M., Gorte, B., 2016. On the performance of remote sensing time series reconstruction methods – a spatial comparison. *Remote Sens. Environ.* 187, 367–384.
- Zhou, H., Yue, X., Lei, Y., Zhang, T., Tian, C., Ma, Y., Cao, Y., 2021. Responses of gross primary productivity to diffuse radiation at global FLUXNET sites. *Atmos. Environ.* 244, 117905.